51st European Rotorcraft Forum
Thursday, September 11, 2025, 13:30-14:00

Airfoil Optimization and 3D Rotor Aerodynamics Exploration for Mars Helicopter using Direct Numerical Simulation

Seongjoong Park[1*], Gunther Wilke[2], Yoonpyo Hong[2], Kwanjung Yee[1]

[1]Seoul National University, South Korea

[2]German Aerospace Center (DLR), Germany

SEOUL NATIONAL UNIVERSITY
AEROSPACE VEHICLE DESIGN LABORATORY

Contents

- Introduction
- Numerical Simulation Setup and Validation
- Optimization Framework
- Optimization Results
- 3D Rotor Aerodynamics with Optimized Airfoils
- Conclusion

Introduction

Introduction

- **Motivation for developing Mars Airborne Explorer (MAE)**
  - Contributing to the realization of South Korean government's goal of developing a domestic Mars exploration vehicle by 2045

Can be achieved by exploring pit crater

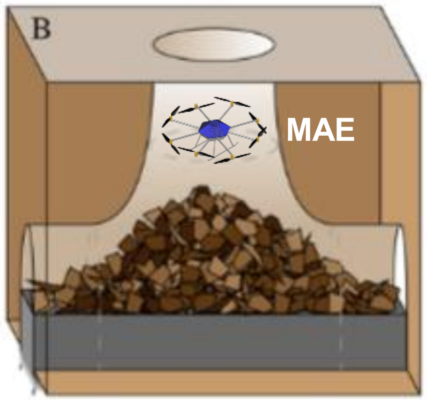

▲ Schematic view of pit crater on Mars

  - **The Mars Airborne Explorer (MAE)** has been developed for pit crater exploration on Mars by conceptual design
  - **MAE frequently undergoes hovering** during its exploration missions
  - Enhancing hovering performance is crucial to increasing the endurance of MAE

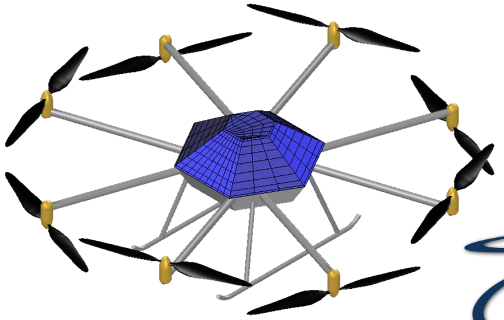

[1 Kim, J. et al., "Object-oriented framework for aircraft conceptual and preliminary design - part I. Architecture and applications," Asia Pacific International Symposium On Aerospace Technology (APISAT), 2024

Introduction

- **Conceptual Design Results of Mars Airborne Explorer (MAE)**
  - Performed by RISPECT III (Rotorcraft Initial Sizing and Performance Estimation Toolkits III)[1]

	Gross weight [kg]	Endurance [min]	Battery capacity [Wh]	Solar cell area [m^2]	Maximum motor torque [Nm]
Octocopter	**12.3**	**8.0**	269.4	0.99	0.448

Weight breakdown result

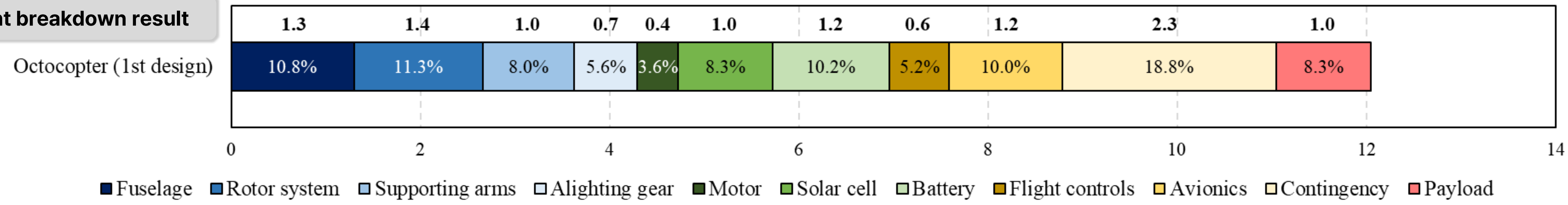

Mission analysis result

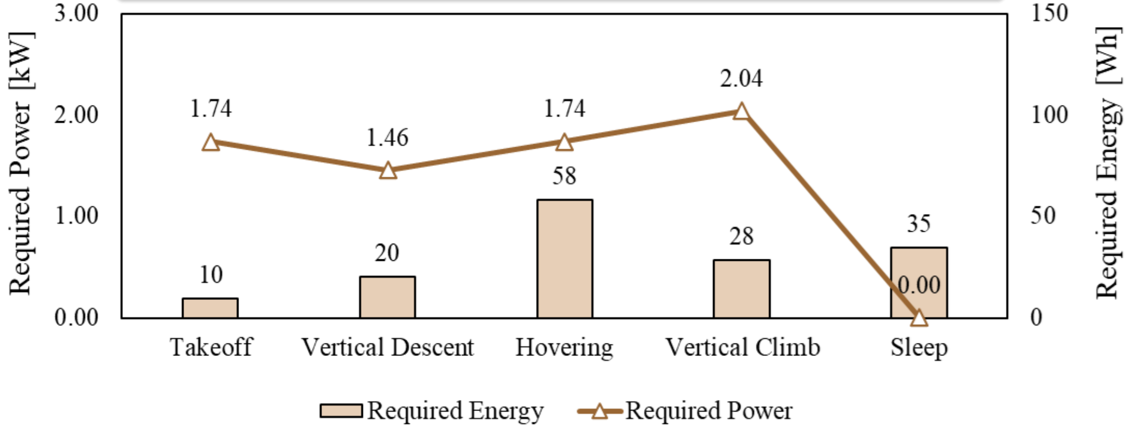

Configuration

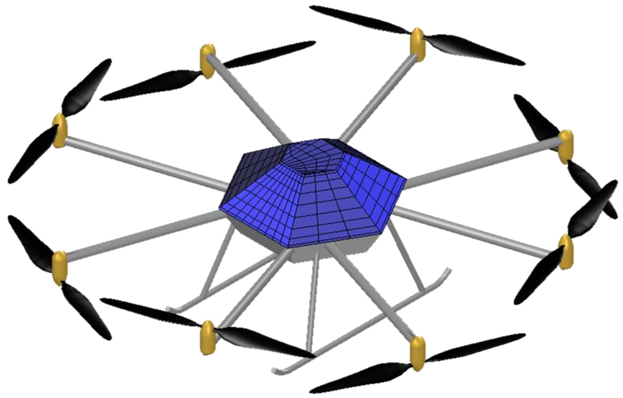

[1] Hassanalian, M. et al., "Evolution of Space Drones for Planetary Exploration: A Review." Progress in Aerospace Sciences, 2018
[2] Wang, S. et al., "Turbulent Intensity and Reynolds Number Effects on an Airfoil at Low Reynolds Numbers," Physics of Fluids, 2014
[3] Sampaio, L. E. B. et al., "The Challenging Case of the Turbulent Flow Around a Thin Plate Wind Deflector, and its Numerical Prediction by LES and RANS Models," Journal of Wind Engineering and Industrial Aerodynamics, 2014

Introduction

- **Requirements for airfoil design optimization**
  - **Objective**: Enhance aerodynamic performance in hover through airfoil shape optimization
  - **Atmospheric Characteristics of Mars**
    - ✓ **Extremely low air density : 1.6% of Earth[1]** → Low Renolds number
    - ✓ Mainly composed of CO_2 (95 %) with small amount of other gases → **Low speed of sound : 240 m/s (70% of Earth)[1]**
  - **Aerodynamic Implications in Martian Atmosphere**
    - ✓ **Low Renolds number → Dominant viscous effects,** large-scale flow structures, and separation bubble behavior
    - ✓ **Low speed of sound → Higher local Mach numbers, leading to increased compressibility effects**

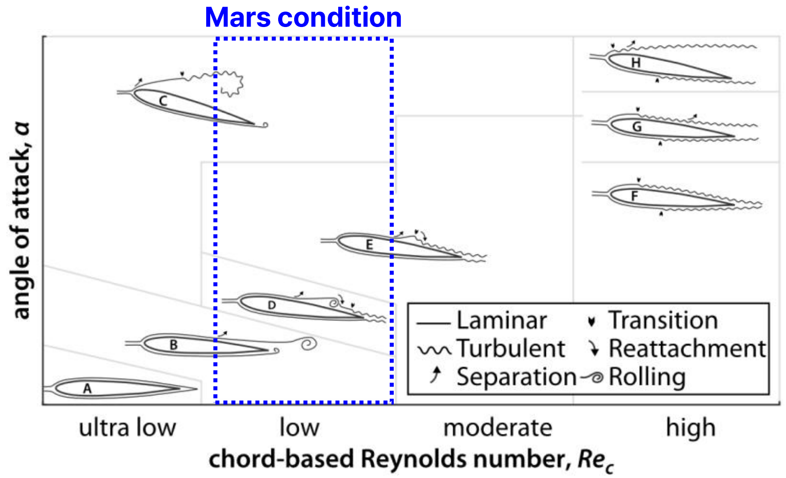

▲ Schematic of flow structures around NACA 0012 airfoil for each Reynolds number regime[2]

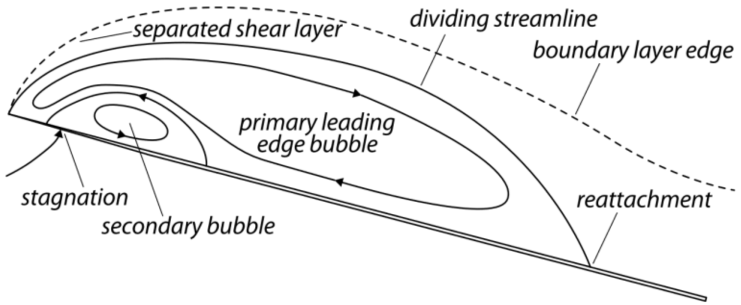

▲ Sketch of leading edge separation bubble on a flat plate[3]

New airfoil shapes must be investigated to cope with low Reynolds number condition

Introduction

[1] Koning, W. J. F. et al., "Performance Optimization of Plate Airfoils for Martian Rotor Applications Using a Genetic Algorithm," 45th European Rotorcraft Forum, 2019
[2] Koning, W. J. F. et al., "Optimization of Low Reynolds Number Airfoils for Martian Rotor Applications Using an Evolutionary Algorithm," AIAA SciTech, 2020
[3] Sasaki, G. et al., "Multi-Objective Optimization of Airfoil for Mars Exploration Aircraft Using Genetic Algorithm," TRANSACTIONS OF THE JAPAN SOCIETY FOR AERONAUTICAL AND SPACE SCIENCES, 2014
[4] Kwon, S. et al., "Aerodynamic Performance of an Arrow Airfoil in Mars Environment and Its Optimization," 47th European Rotorcraft Forum, 2021
[5] Caros, L. et al., "Optimization of Triangular Airfoils for Martian Helicopters Using Direct Numerical Simulations," AIAA Journal, 2023
[6] Koning, W. J. F. et al., "ELISA: A Tool for Optimization of Rotor Hover Performance at Low Reynolds Number in the Mars Atmosphere," Journal of the American Helicopter Society, 2024.
[7] Koning, W. J. F. et al., "Overview of Rotor Hover Performance Capabilities at Low Reynolds Number for Mars Exploration.", 50th European Rotorcraft Forum, 2024

- **Previous Research on Airfoil Optimizations for Low Reynolds number**
  - **Single/Multi-objective airfoil optimization using Unsteady Reynolds-Averaged Navier-Stokes (URANS) [1-4]**
    - ✓ Limitation: RANS simulations rely on turbulence models that approximate small-scale turbulent structures, making them **insufficient for accurately capturing large-scale flow structures and separation bubble behavior in low Reynolds number environments**
  - **Airfoil optimization using Direct Numerical Simulation (DNS) [5-6]**
    - ✓ Limitation: Since these airfoils were designed based on 2D simulations, **it is necessary to verify whether their optimized performance is retained when applied to 3D rotor blade**
  - **3D rotor analysis with optimized airfoils using a free wake model-based comprehensive analysis code [7]**
    - ✓ Limitation: Because of the highly unsteady flow in low Reynolds number environment, it is need to analyze the rotor with high-fidelity CFD simulation
  - **Analyzed the enhanced performance of the optimized airfoil based on the same angle of attack or L/D [1-7]**
    - ✓ Limitation: Lack of detail comparison between their performance under thrust-trimmed condition

1. Perform 3D rotor CFD analysis with optimized airfoil
2. Identify detail mechanism of their superior performance under thrust-trimmed condition

Introduction

[1] Koning, W. J. F. et al., "Performance Optimization of Plate Airfoils for Martian Rotor Applications Using a Genetic Algorithm," 45th European Rotorcraft Forum, 2019
[2] Koning, W. J. F. et al., "Optimization of Low Reynolds Number Airfoils for Martian Rotor Applications Using an Evolutionary Algorithm," AIAA SciTech, 2020
[3] Sasaki, G. et al., "Multi-Objective Optimization of Airfoil for Mars Exploration Aircraft Using Genetic Algorithm," TRANSACTIONS OF THE JAPAN SOCIETY FOR AERONAUTICAL AND SPACE SCIENCES, 2014
[4] Kwon, S. et al., "Aerodynamic Performance of an Arrow Airfoil in Mars Environment and Its Optimization," 47th European Rotorcraft Forum, 2021
[5] Caros, L. et al., "Optimization of Triangular Airfoils for Martian Helicopters Using Direct Numerical Simulations," AIAA Journal, 2023
[6] Koning, W. J. F. et al., "ELISA: A Tool for Optimization of Rotor Hover Performance at Low Reynolds Number in the Mars Atmosphere," Journal of the American Helicopter Society, 2024.
[7] Koning, W. J. F. et al., "Overview of Rotor Hover Performance Capabilities at Low Reynolds Number for Mars Exploration.", 50th European Rotorcraft Forum, 2024

- Previous Research on Airfoil Optimizations for Low Reynolds number
  - Sin… NS) [1-4]
    - ✓ L… m insufficient for accurately capturing large-scale flow structures and separation bubble behavior in low Reynolds number environments
  - …sing Direct Numerical Simulation (DNS) [5-6]
    - … CFD simulation
  - Analyzed the enhanced performance of the optimized airfoil based on the same angle of attack or L/D [1-7]
    - ✓ Limitation: Lack of detail comparison between their performance under thrust-trimmed condition

1. Perform 3D rotor CFD analysis with optimized airfoil
2. Identify detail mechanism of their superior performance under thrust-trimmed condition

Research Objectives

- Derive optimized airfoils that outperform baseline airfoils under Mars flight conditions using DNS
- **Identify the detail mechanism** behind the superior performance of the optimized airfoils under thrust-trimmed condition
- **Investigate 3D rotor aerodynamics with the optimized airfoil,** comparing it to the baseline rotor using DNS

Aerospace Vehicle Design Laboratory

Numerical Simulation Setup and Validation

[1] Raddatz J. et al., "Block Structured Navier-Stokes Solver FLOWer," MEGAFLOW - Numerical Flow Simulation for Aircraft Design, 2005

2D Numerical Simulation Setup

- **Numerical simulation setup for 2D FLOWer**
  - 2D Direct Numerical Simulation (DNS)

Solver Details	
Solver	FLOWer[1]
Spatial Discretization Scheme	SLAU2 scheme (upwind), 3rd order van Albada limiter
Time Integration Scheme	Physical time : BDF2 $\Delta t = 1/305\, ctu$, $50\, ctu$ run = 15250 time steps Pseudo time: 2nd order Runge-Kutta (target residual = 10^{-5}, max iter. = 100)
Turbulence Model	No turbulence model

Grid Details	
Grid Type	O-grid
Minimum cell height	y+ < 1
Chordwise	609
Normal	120
Total number of cells	73,000

*ctu: convection time unit $(1ctu = 1/M_{\infty})$

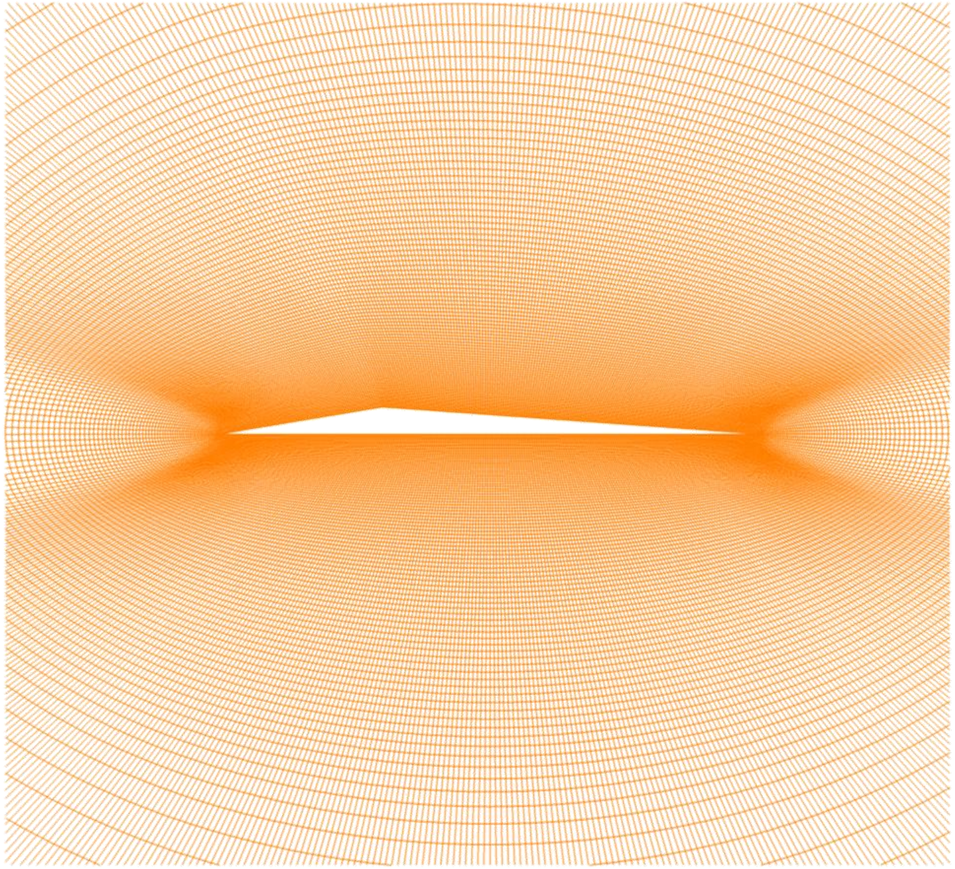

▲Typical grid of triangular airfoil used for simulation

[1] Raddatz J. et al., "Block Structured Navier-Stokes Solver FLOWer," MEGAFLOW - Numerical Flow Simulation for Aircraft Design, 2005
[2] Wilke, G., "G-cube (Gunther's Grid Generator)"
[3] Koning, W. J. F. et al., "Comparing 3D and 2D CFD for Mars Helicopter Ingenuity Rotor Performance Prediction," presented at the 49th European Rotorcraft Forum, 2023
[4] Chaderjian, N. M., "Quantitative Approach for the Accurate CFD Simulation of Hover in Turbulent Flow." International Conference on Computational Fluid Dynamics, 2022

3D Numerical Simulation Setup

- **Numerical simulation setup for 3D FLOWer**
  - 3D Direct Numerical Simulation (DNS)

Solver Details	
Solver	FLOWer[1]
Spatial Discretization Scheme	SLAU2 scheme (upwind), 4th order van Albada limiter
Time Integration Scheme	Physical time : BDF2 $\Delta t = 0.25°$ for last 5 revs / $\Delta t = 1°$ for initial 25 revs Pseudo time: BDF1 (CFL # = 10, Target residual = 10^{-5}, max iter. = 100) Matrix inversion: LU-SGS
Turbulence Model	No turbulence model

Grid Details	Generated by G-cube[2]
Grid Type	O-O grid
Minimum cell height	y+ < 1
Blade mesh cells	16.9 M (chordwise: 513, normal: 129, spanwise: 256)
Farfields/outer grid cells	67.6 M (periodic mesh)
Total number of cells	84.5 M

Similar grid parameter with previous research[3, 4]

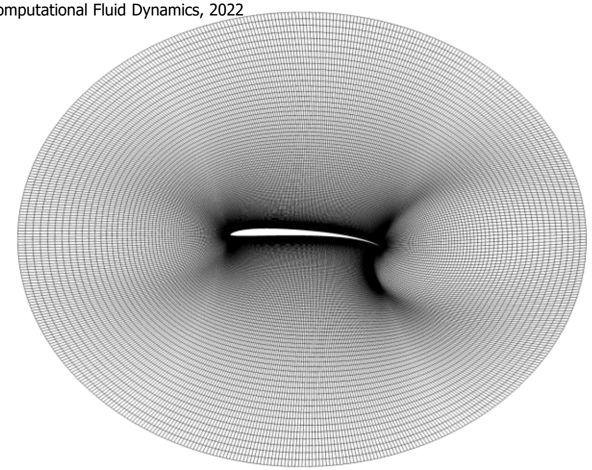

▲Grid topology of airfoil section

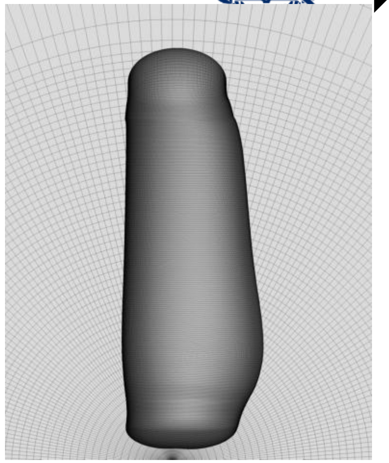

▲O-O type blade grid

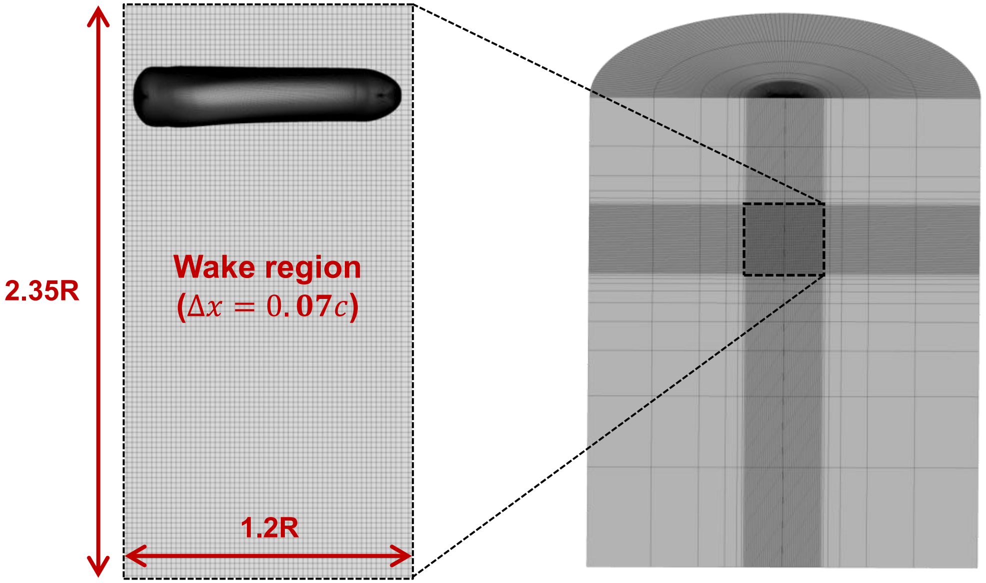

▲Wake grids and overall background grids for 3D CFD hover calculations

2D/3D Validation Results

[1] Munday, P. M. et al., "Nonlinear lift on a triangular airfoil in low-Reynolds-number compressible flow," Journal of Aircraft, 2015
[2] Koning, W. J. F. et al., "Optimization of Low Reynolds Number Airfoils for Martian Rotor Applications Using an Evolutionary Algorithm," AIAA SciTech, 2020
[3] Caros, L. et al., "Direct Numerical Simulation of Flow over a Triangular Airfoil Under Martian Conditions," AIAA Journal, 2022
[4] Koning, W. J. F. et al., "Comparing 3D and 2D CFD for Mars Helicopter Ingenuity Rotor Performance Prediction," 49th European Rotorcraft Forum, 2023

2D Validation result

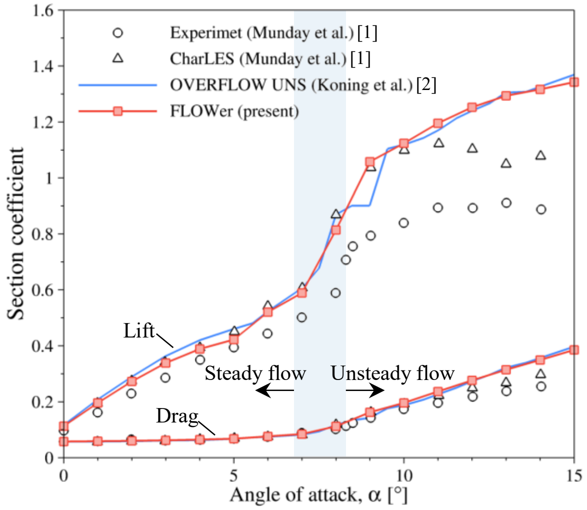

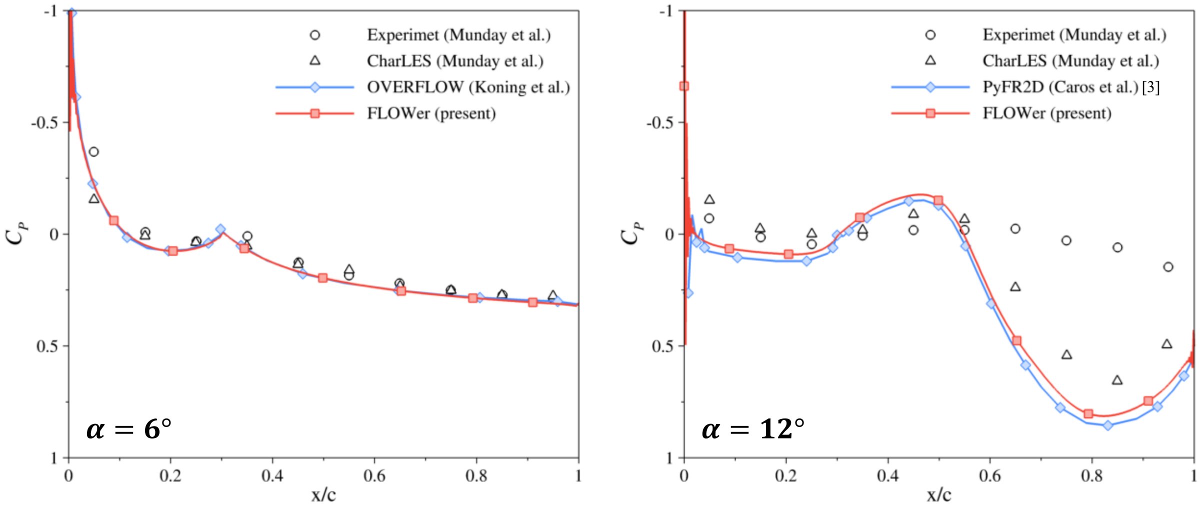

▲ Pressure coefficient Cp on the Suction surface of airfoil (time-averaged)

3D Validation result

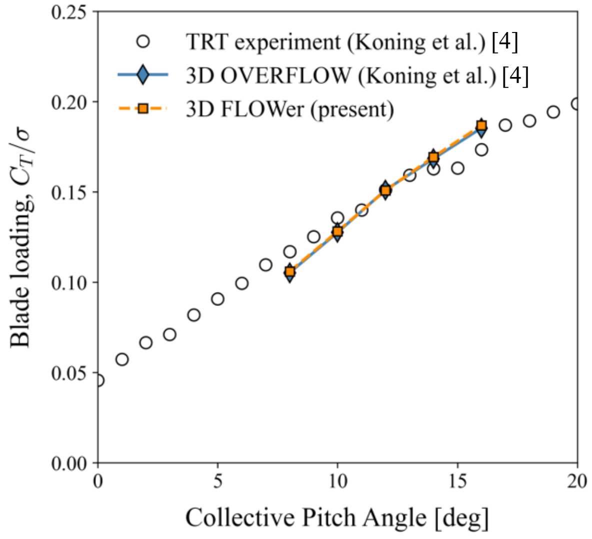

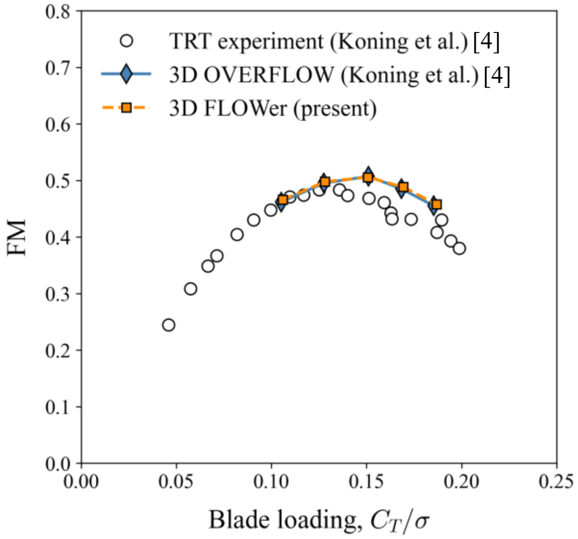

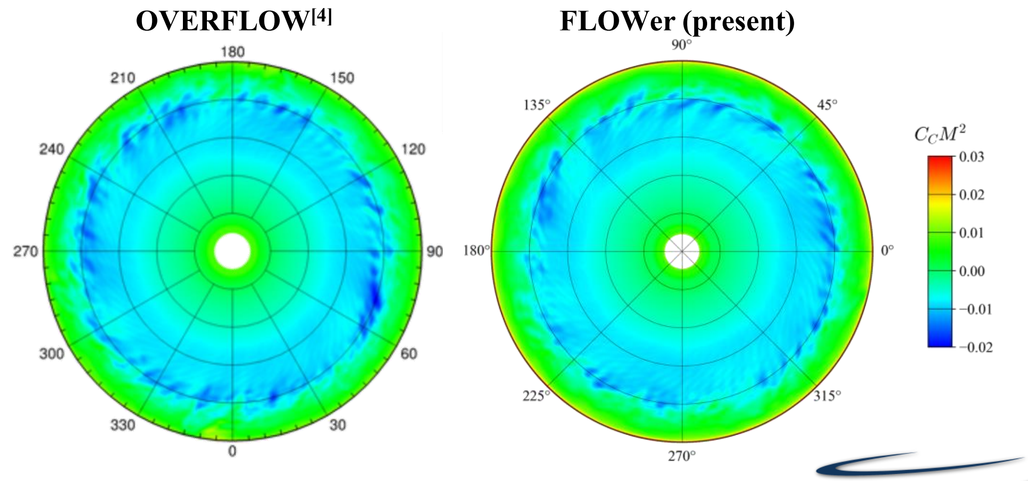

▲ Rotor sectional axial (chord) force coefficient

Aerospace Vehicle Design Laboratory

Optimization Framework

[1] Wilke, G., "POT (Powerful Optimization Tools with Surrogate Modeling)"
[2] Wilke, G., "Variable-Fidelity Methodology for the Aerodynamic Optimization of Helicopter Rotors," AIAA Journal, 2019
[3] Krige, D. G., "A Statistical Approach to Some Mine Valuation and Allied Problems on the Witwatersrand," PhD thesis, 2015
[4] Storn, R. et al., "Differential Evolution – A Simple and Efficient Heuristic for Global Optimization over Continuous Spaces," Journal of Global Optimization, 1997
[5] Hooke, R. et al., " "Direct Search" Solution of Numerical and Statistical Problems," J. ACM, 1961

Optimization Framework

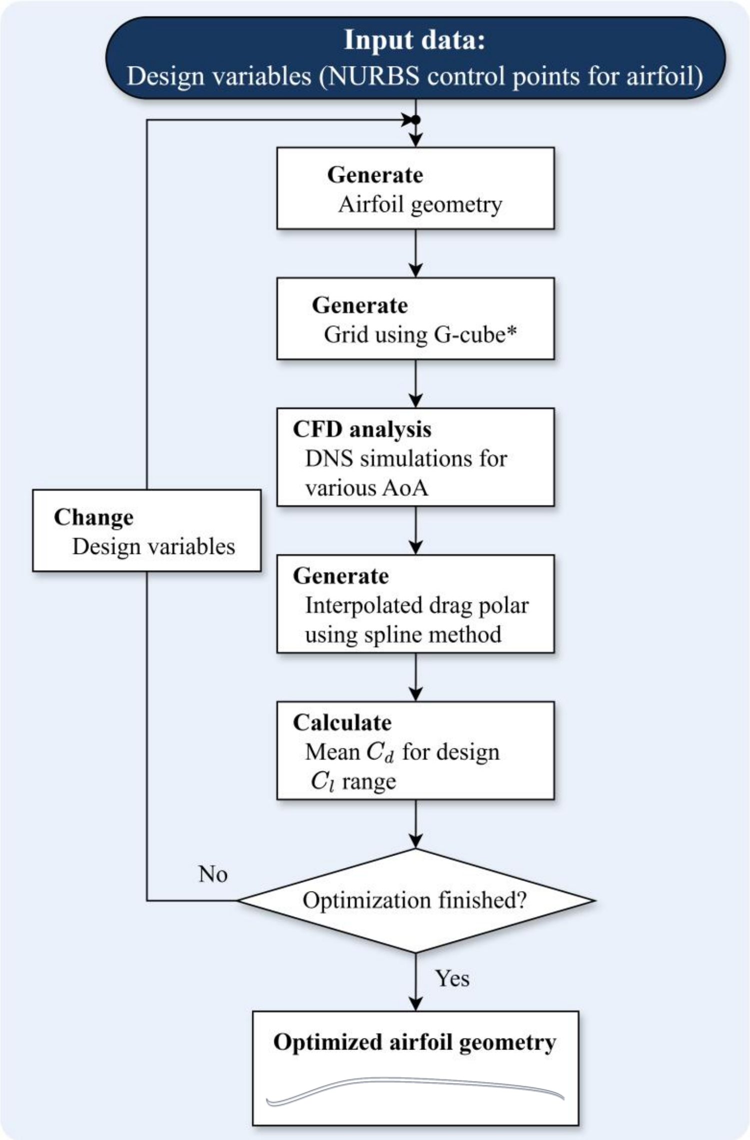

▲ Overall optimization process

- **Efficient Global Optimization (EGO) Framework (POT)[1, 2]**
  - Design of experiment : Central Voronoi Tessellation (CVT)
  - Surrogate modeling : Kriging[3]
    - ✓ Combination of a trend function (polynomial regression model) and radial basis function (RBF) approximation of the error

$$\hat{y}(\vec{x}) = \hat{f}_{trend}(\vec{x}) + \hat{\epsilon}_{rbf}(\vec{x}) \Longrightarrow \hat{\boldsymbol{y}}(\vec{\boldsymbol{x}}) = \hat{\boldsymbol{f}}_v(\vec{\boldsymbol{x}})\vec{\boldsymbol{\beta}} + \hat{\boldsymbol{\psi}}_v(\vec{\boldsymbol{x}})\vec{\boldsymbol{W}}$$

$$(\vec{\beta}: polynomial\ coefficient\ vector, \hat{\psi}_v: correlation\ vector, \vec{W}: weight\ vector)$$

  - Optimizer : Differential Evolutionary algorithm (DE)[4] + Hooke and Jeeves[5]
    - ✓ One dimension of the trial vertor of DE :

$$\vec{v}_i = \vec{x}_t + F(\vec{x}_r - \vec{x}_s) \quad (r, s, t: arbitrary\ random\ integers, F: scaling\ factor)$$

	Value
Number of Initial samples	150 points
Number of improvement cycles	8 updates with 4 points
Number of optimization cycles	8 iterations

▲ Description of the optimization framework setup

*G-cube : Gunther's Grid Generator

Optimization Framework

[1] Lu, X. et al., "An Improved Geometric Parameter Airfoil Parameterization Method," Aerospace Science and Technology, 2018
[2] Wilke, G., "AFRO (Airfoils for Rotor Optimization)"
[3] Koning, W. J. F. et al., "ELISA: A Tool for Optimization of Rotor Hover Performance at Low Reynolds Number in the Mars Atmosphere," Journal of the American Helicopter Society, 2024.

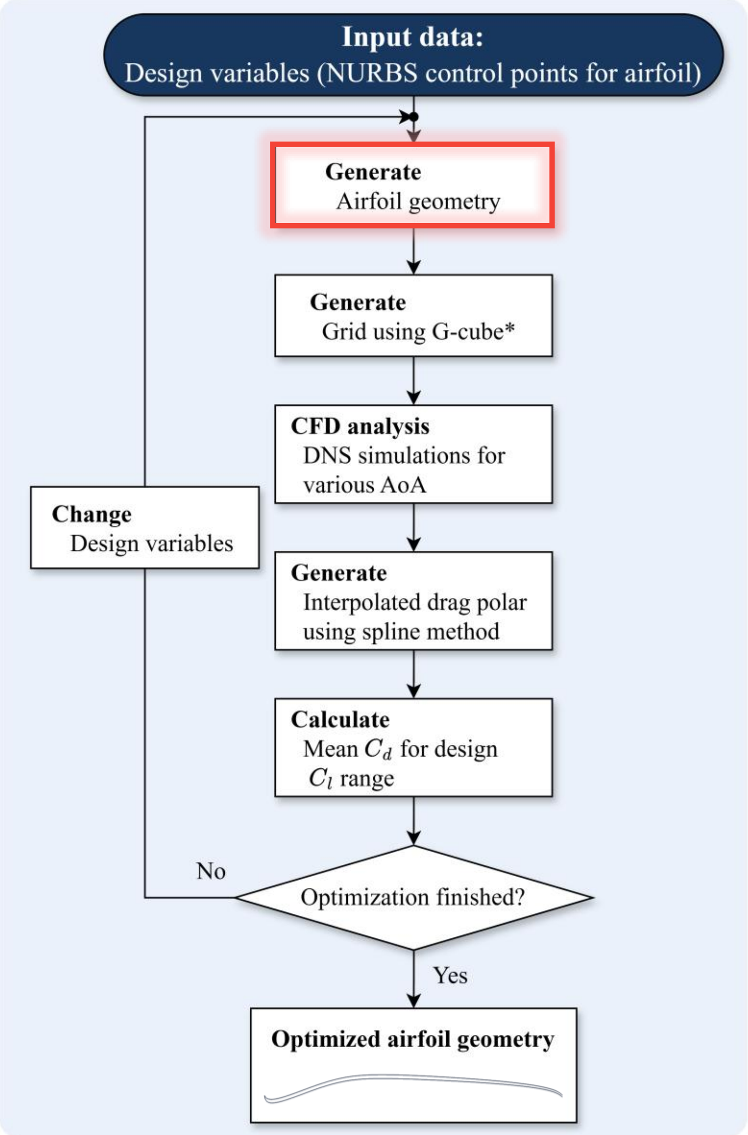

▲ Overall optimization process

- **Parameterization Method**
  - Improved geometric parameterization (IGP) with *NURBS[1, 2]
    - ✓ Camber line expressed by NURBS with 6 control points : $c_i(x_i, y_i)$
    - ✓ Thickness line expressed by NURBS with 6 control points : $t_i(x_i, y_i)$
    - ✓ Can cover every geometries generated by other parameterization method ex) Bezier curve[3], etc.

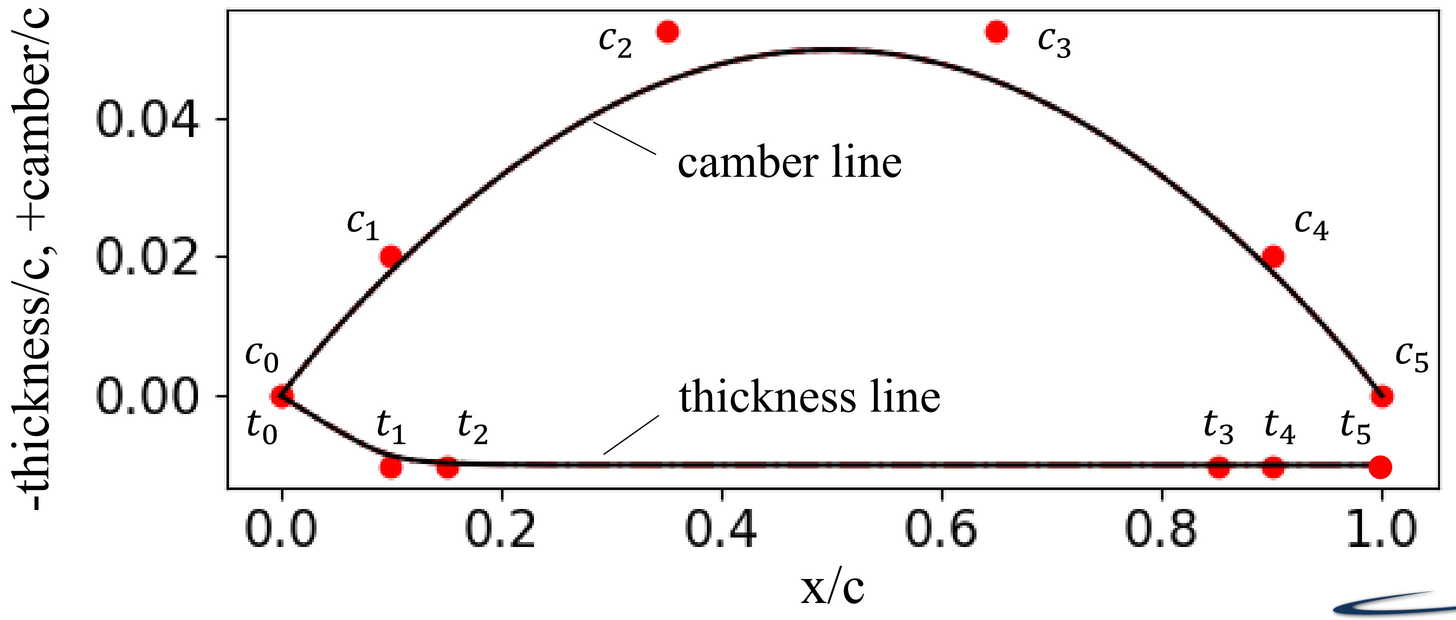

▲ Definition of NURBS for decoupled camber and thickness

*NURBS: Non-uniform rational B-spline

Optimization Framework

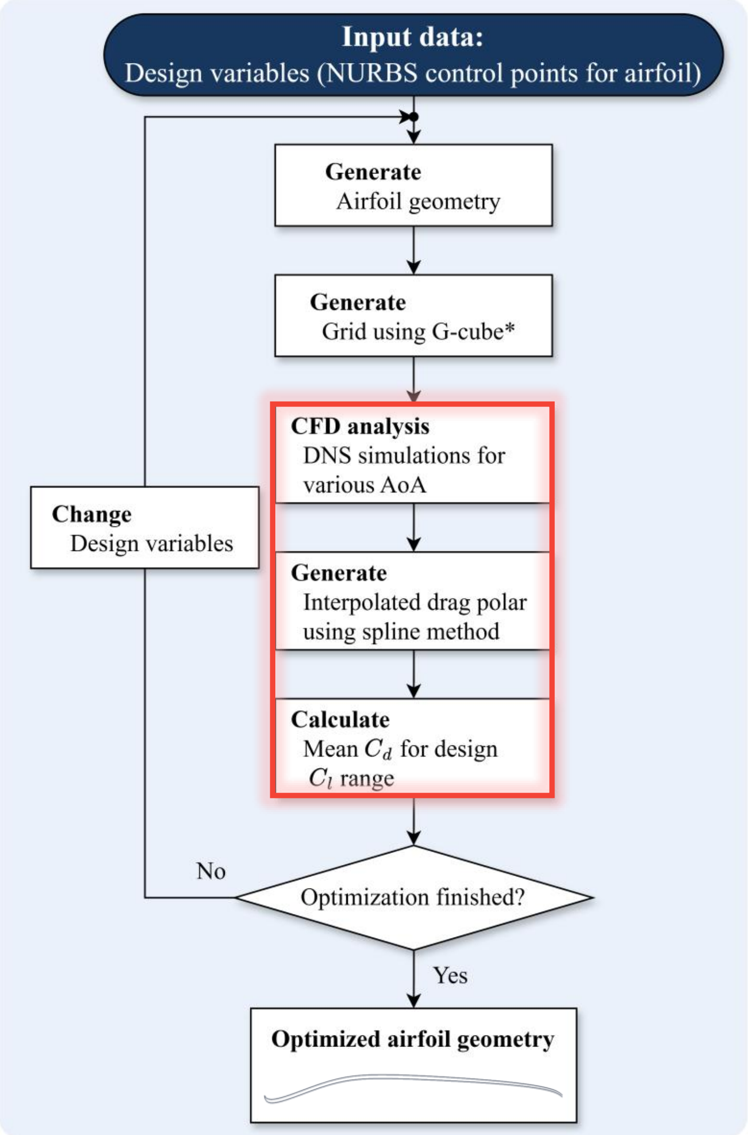

▲ Overall optimization process

- **Evaluation of Objective Function**
  - Objective function : ***minimize*** $c_{d_{mean}}$
  - Calculation process for $c_{d_{mean}}$

1. CFD analysis 2. Generate interpolated drag polar 3. Calculate mean $c_{d_{mean}}$

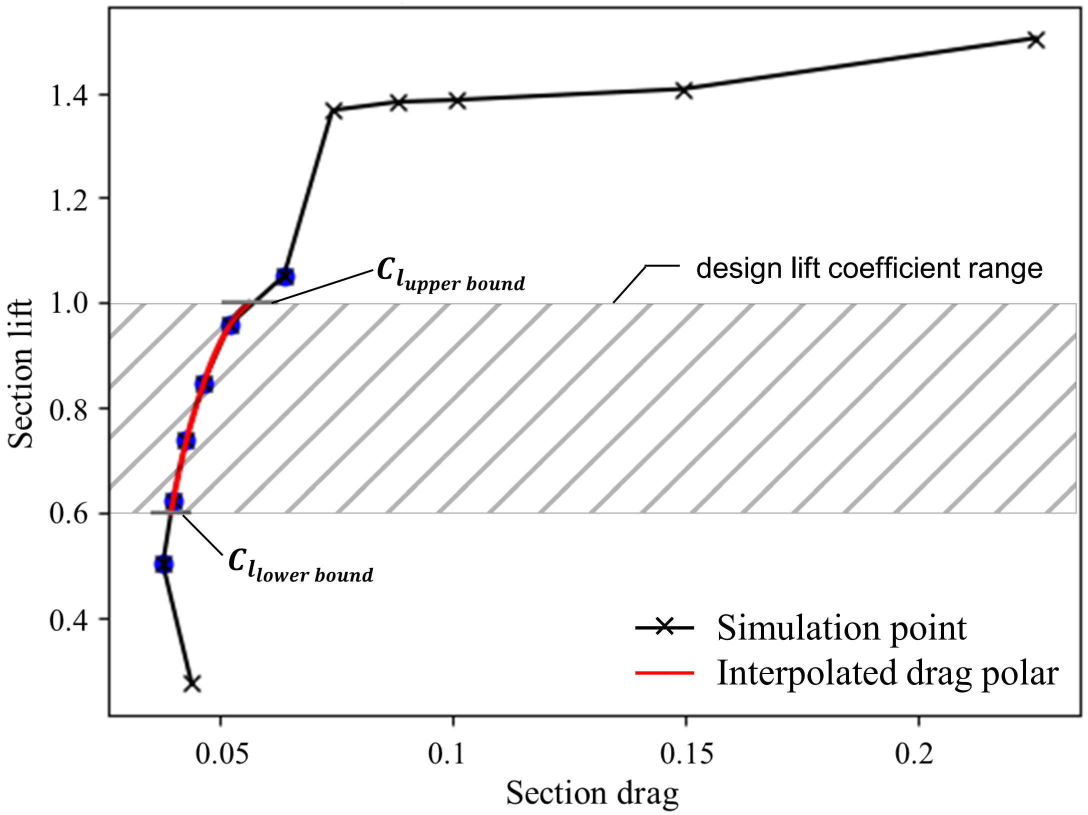

[1] Koning, W. J. F. et al., "Mars Helicopter Ingenuity Rotor Geometry," NASA/TM-20240001510, 2024

Optimization Task

- **Single-Objective Efficient Global Optimization (EGO)**
  - Objective function : $\boldsymbol{minimize\ c_{d_{mean}}}$
  - Constraint : $t/c_{min} > t/c_{min,\ baseline}$

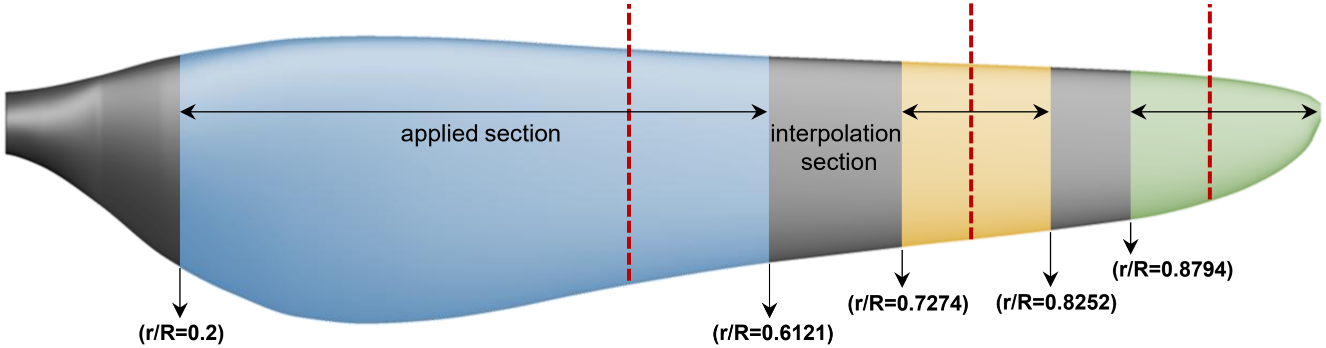

Target thrust = 7.35 N $(C_T/\sigma = 0.125)$
(required thrust for hovering derived from conceptual design)

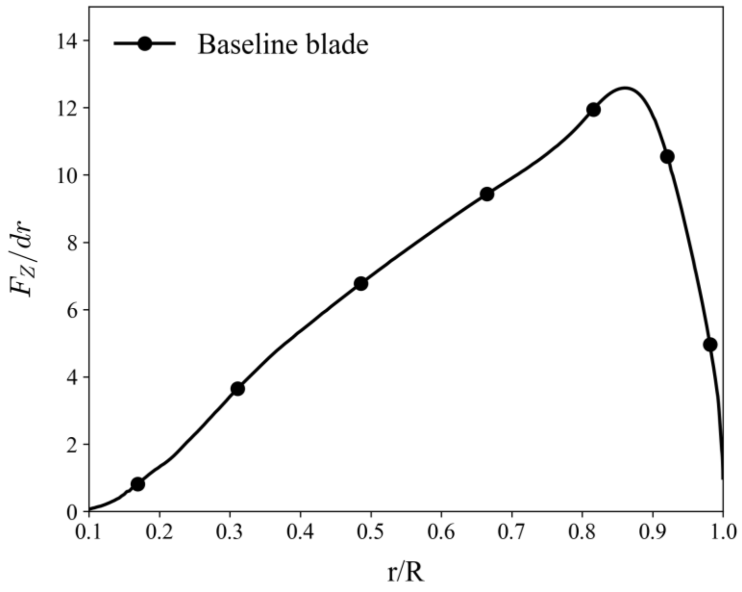

▲ Sectional load distribution of baseline blade in hover

Derive operation conditions (C_l)

Station	r/R	Re_c	$Mach$	$C_{l_{lower\ bound}}$	$C_{l_{upper\ bound}}$	$^*t/c_{min,baseline}$
1	0.5271	13790	0.40	0.6	1.0	0.51 %
2	0.7520	14845	0.58	0.55	0.95	0.68 %
3	0.9241	12822	0.70	0.45	0.85	0.96 %

▲ Flow condition and evaluation range for fitness value ($c_{d_{mean}}$) of each Station

*thickness constraints are derived from OML CAD model of Ingenuity's rotor blade [1]

Optimization Task

- **Single-Objective Efficient Global Optimization (EGO)**
  - Number of design variables : 10

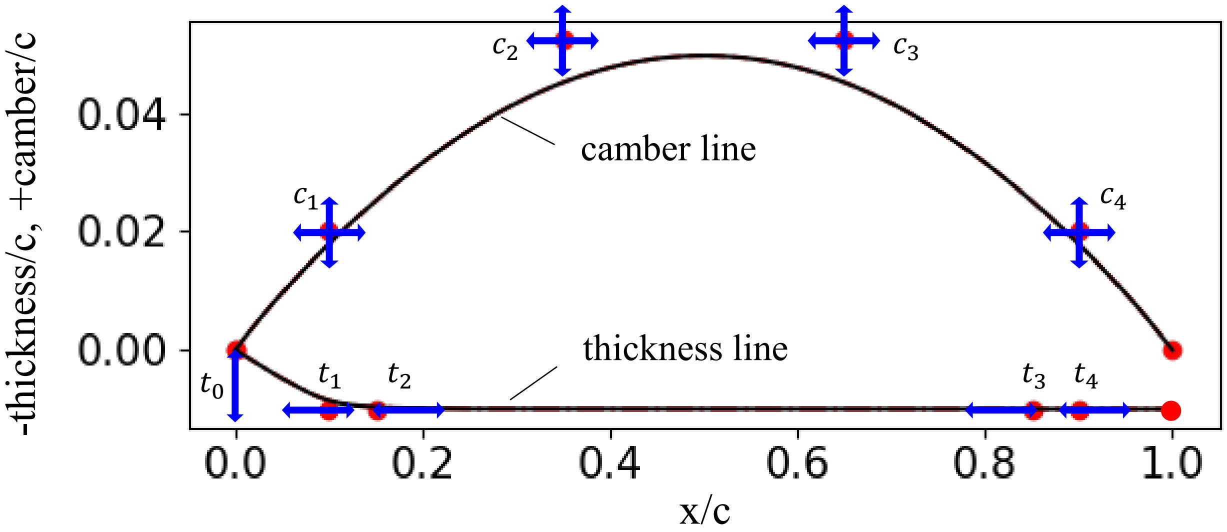

▲ Definition of NURBS for decoupled camber and thickness

Value	Variable	Lower bound	Upper bound
DV_1	$x_1\ for\ c_1$	0.01	0.1
DV_2	$y_1\ for\ c_1$	-0.05	0.05
DV_3	$x_2\ for\ c_2$	0.1	0.4
DV_4	$y_2\ for\ c_2$	0	0.1
DV_5	$x_3\ for\ c_3$	0.4	0.75
DV_6	$x_4\ for\ c_4$	0.75	0.95
DV_7	$y_4\ for\ c_4$	-0.05	0.05
DV_8	$y_0\ for\ t_0$	-0.05	0.05
DV_9	$x_1\ for\ t_1$	-0.05	0.05
DV_{10}	$x_4\ for\ t_4$	-0.05	0.05

  - Baseline : **clf5605 airfoil (TE modified)** of Ingenuity's blade

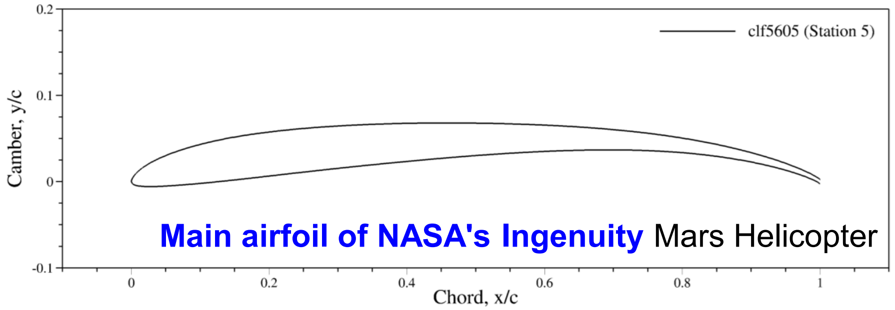

Main airfoil of NASA's Ingenuity Mars Helicopter

Variable	Earth (SLS)	MAE flight condition
Density, ρ [kg/m^3]	1.225	**0.017**
Temeratura, T [K]	288.2	223
Gas constant, R [m^2 /s^2 /K]	287.1	188.9
Specific heat ratio, γ	1.4	1.289
Speed of sound, a [m/s]	340.35	220

▲ Flight condition of Mars Aerial Explorer

Optimization Results

Optimization Results

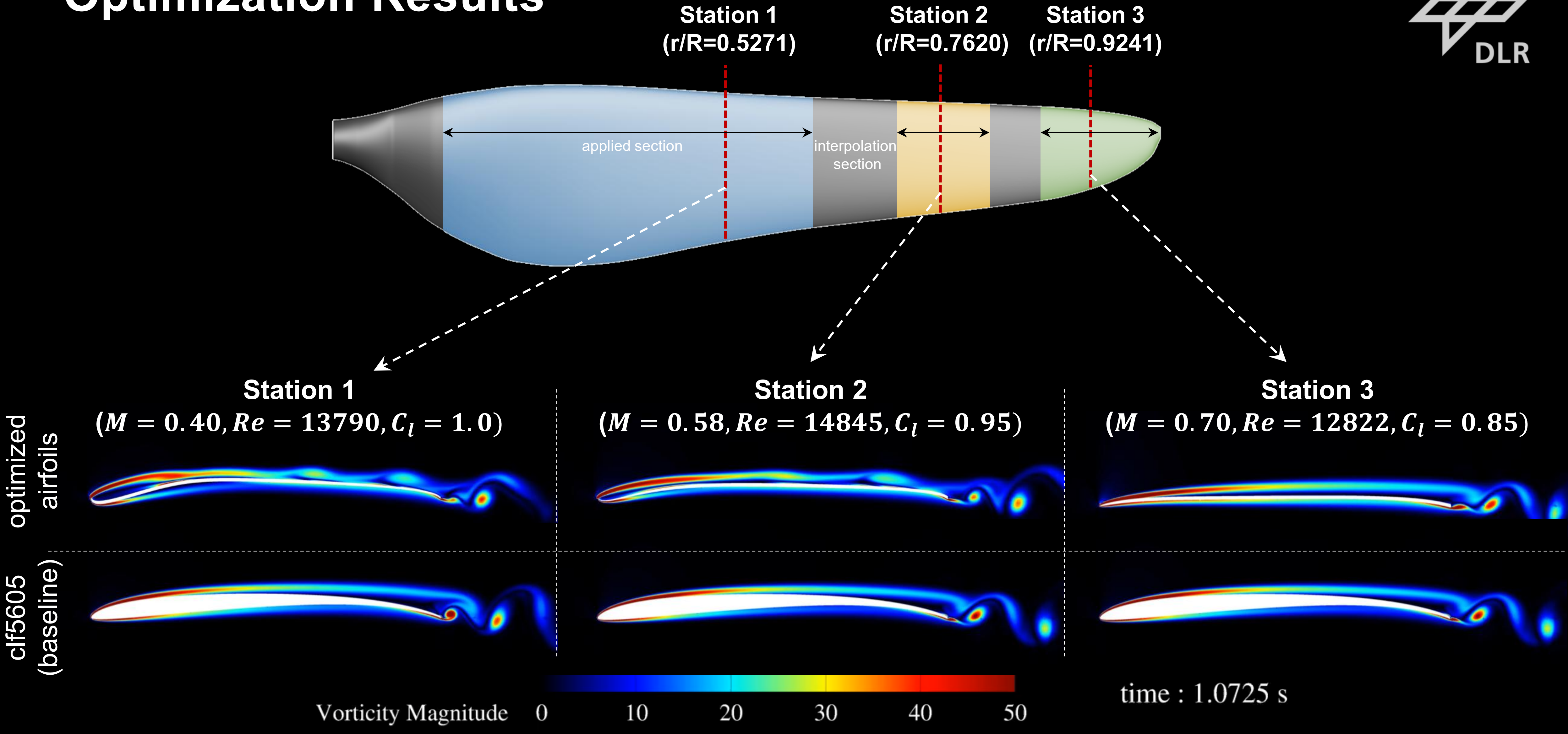

SEOUL NATIONAL UNIVERSITY
AEROSPACE VEHICLE DESIGN LABORATORY

[1] Koning, W. J. F. et al., "ELISA: A Tool for Optimization of Rotor Hover Performance at Low Reynolds Number in the Mars Atmosphere," Journal of the American Helicopter Society, 2024

Optimization Results

- **Flow physics of Sharp Raised Lip (SRL) airfoil**

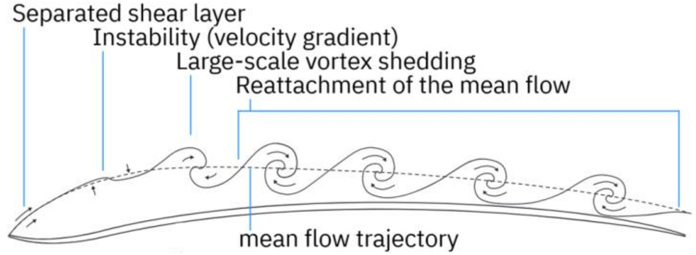

▲ Schematic flow physics over raised-lip LE airfoil [1]

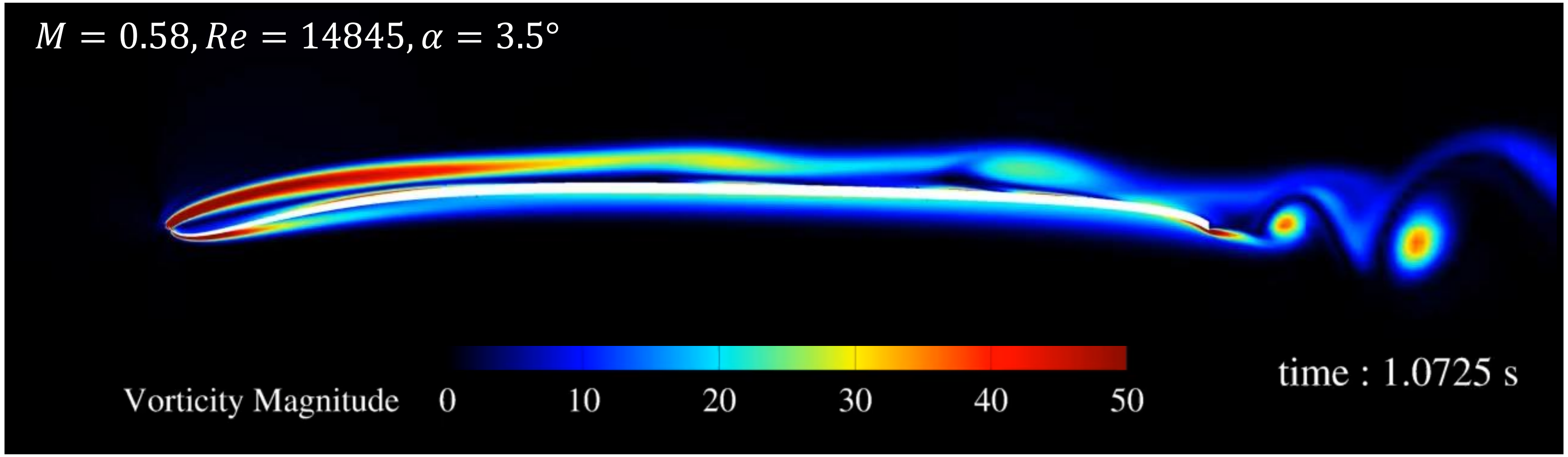

▲ Instantaneous flow field around SRL airfoil

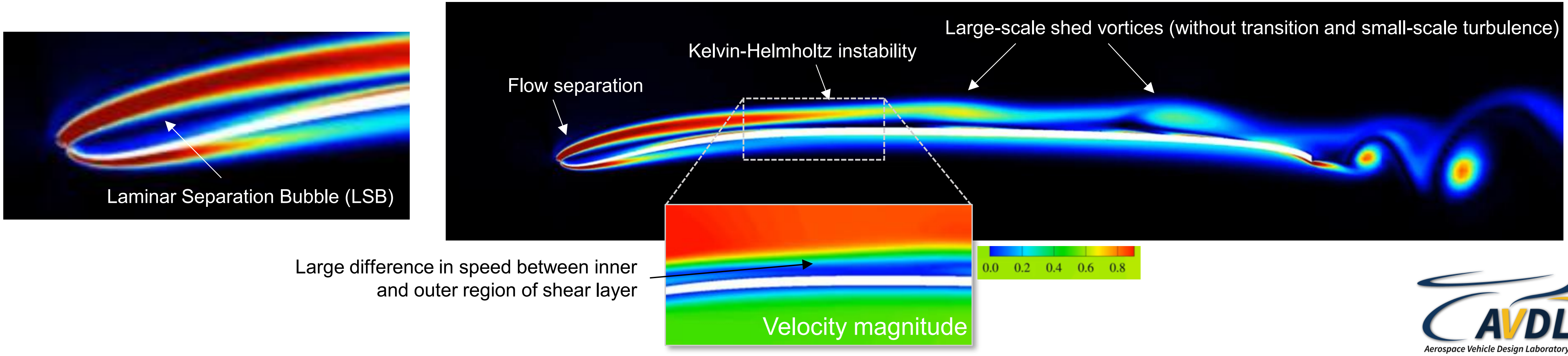

Optimization Results

- **Station 1 ($r/R = 0.5271$)**
  - Optimized airfoil has a **Sharp Raised Lip (SRL)**

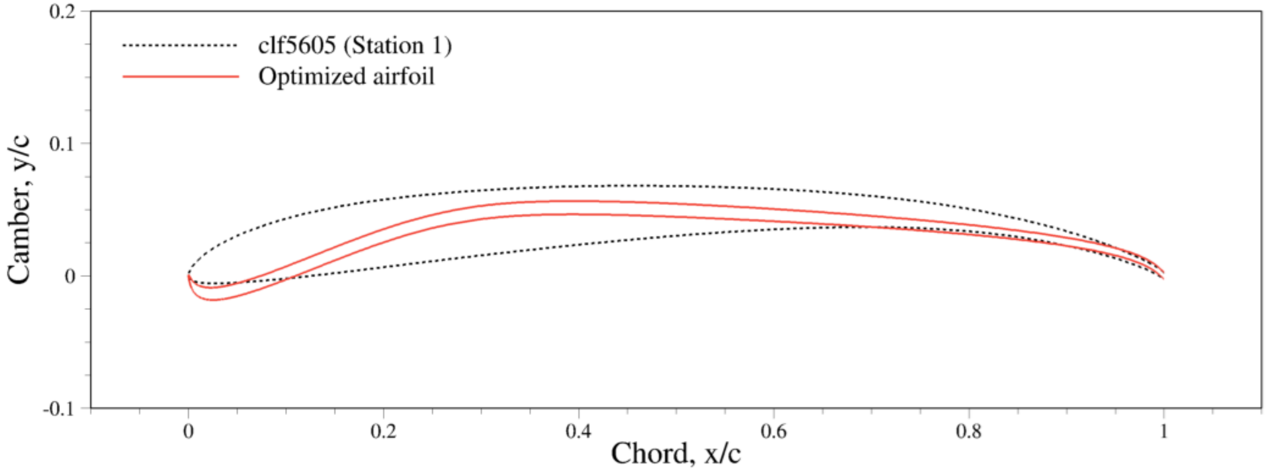

Performance	Fitness ($C_{d_{mean}}$*)	Improvement [%]
clf5605 (baseline)	**0.0455**	
Optimized airfoil	0.0359	21.1

Geometry	Max. Camber (f/c)	Max. Thickness (t/c)	Thickness (t/c) @ TE
clf5605 (baseline)	0.050	0.051	0.005
Optimized airfoil	0.051	0.010	0.005

*range of $C_{d_{mean}}$: $0.6 < C_l < 1.0$

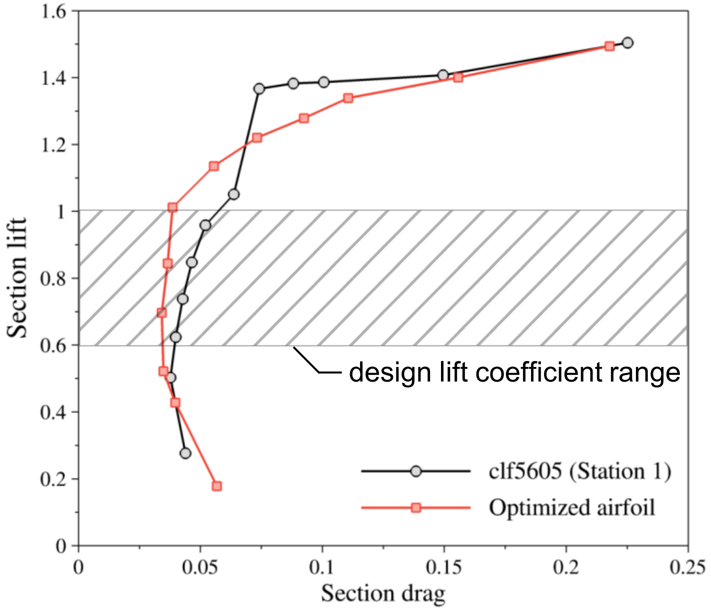

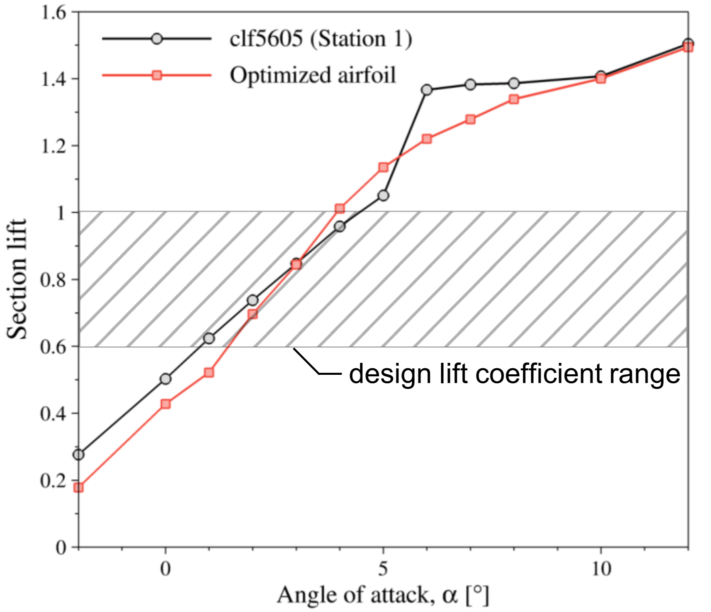

▲ Drag polar and lift curve for $Re = 13790$ and $M = 0.4$

Flow condition : $M = 0.40, Re = 13790$

Optimization Results

$C_{d_{total}} = C_{d_{pressure}} + C_{d_{friction}}$

-14% +51% -68%

Averaged sectional distribution (last 25 ctu)

- **Station 1 ($C_l = 0.6$)**

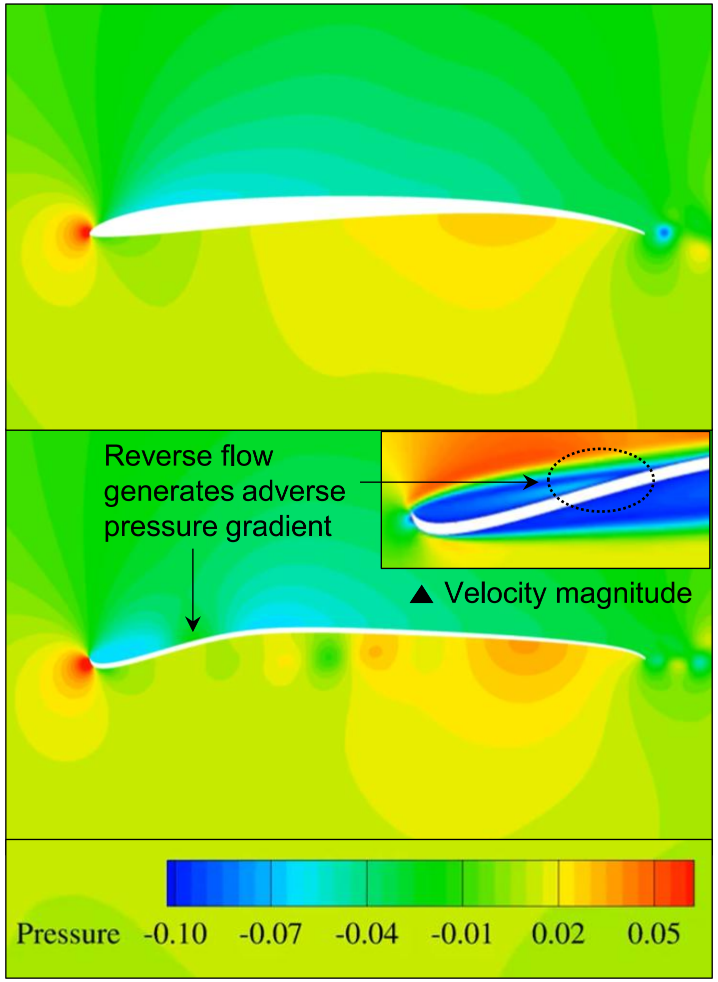

▲ Instantaneous flow field
(non-dimensional gage pressure)

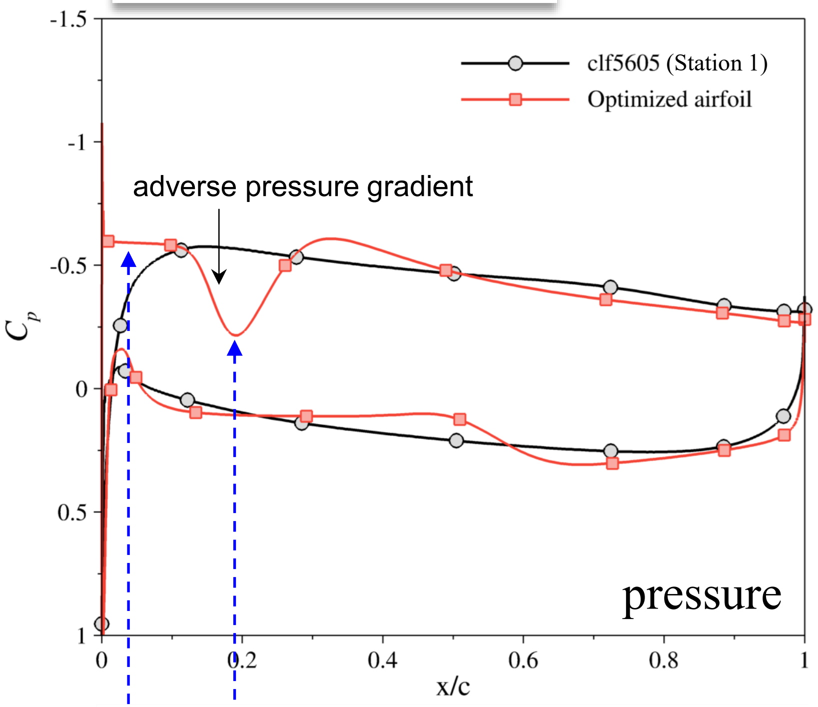

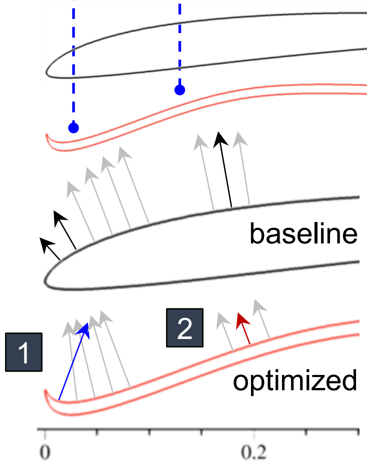

1	Normal force is tilted to direction of drag (∵ reverse camber effect)
2	Pressure is increased (∵ adverse pressure gradient effect)

⇒ ***Higher $C_{d_{pressure}}$***
(compared to baseline)

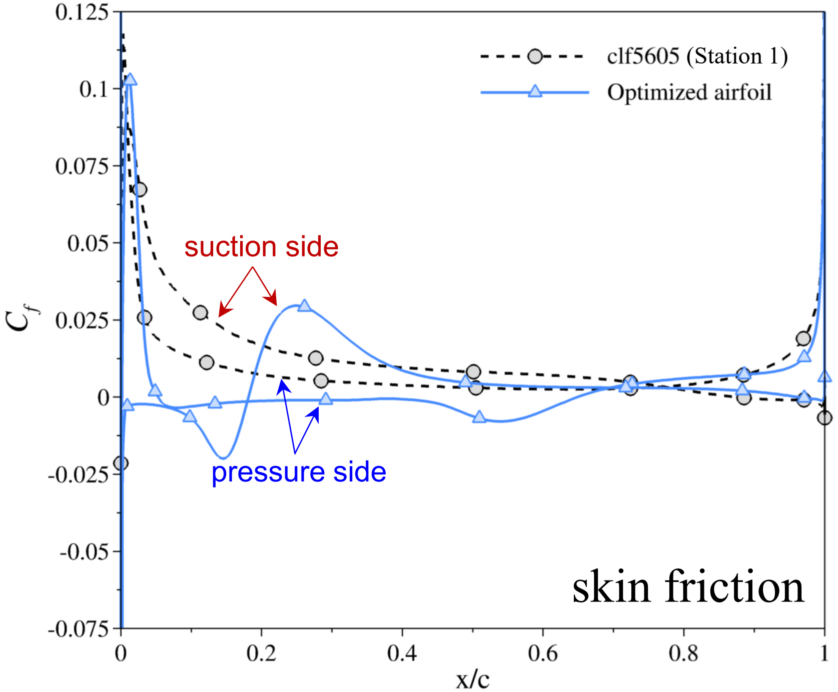

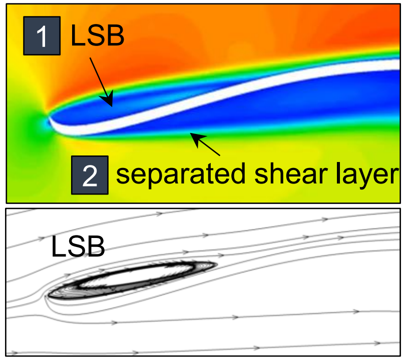

▲ Velocity contour and streamline

1	Lower C_f near LE at suction side (∵ Laminar Separation Bubble (LSB) effect)
2	Lower C_f near $x/c < 0.6$ at pressure side (∵ Shear layer separation)

⇒ ***Lower $C_{d_{friction}}$***
(compared to baseline)

AVDL Aerospace Vehicle Design Laboratory

Flow condition : $M = 0.58, Re = 14845$

Optimization Results

- **Station 2 ($r/R = 0.762$)**
  - Optimized airfoil has a **Sharp Raised Lip (SRL)**

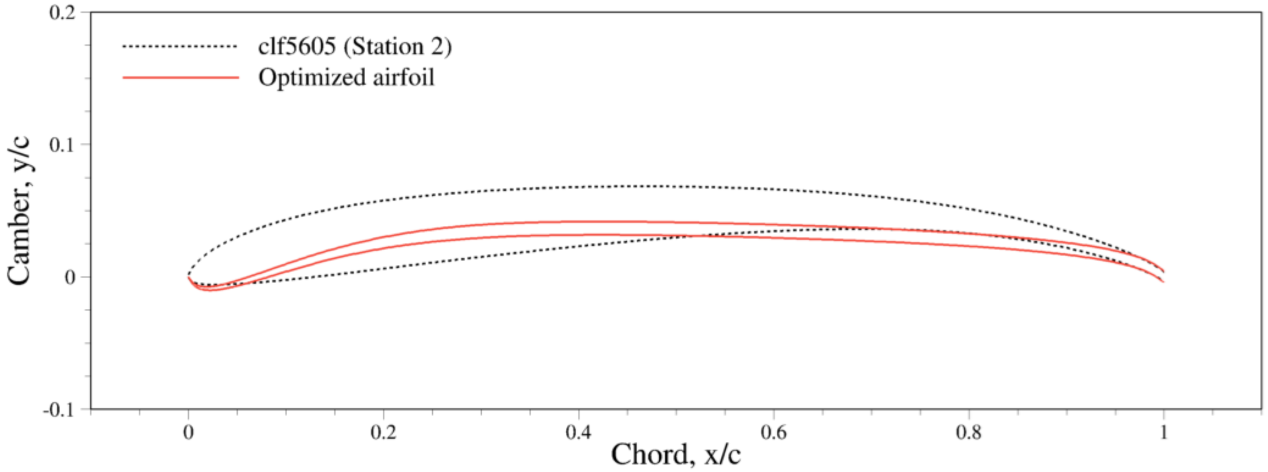

Performance	Fitness ($C_{d_{mean}}$*)	Improvement [%]
clf5605 (baseline)	**0.0458**	
Optimized airfoil	**0.0344**	**24.8**

Geometry	Max. Camber (f/c)	Max. Thickness (t/c)	Thickness (t/c) @ TE
clf5605 (baseline)	0.050	0.051	0.007
Optimized airfoil	0.037	0.010	0.009

*range of $C_{d_{mean}}$: $0.55 < C_l < 0.95$

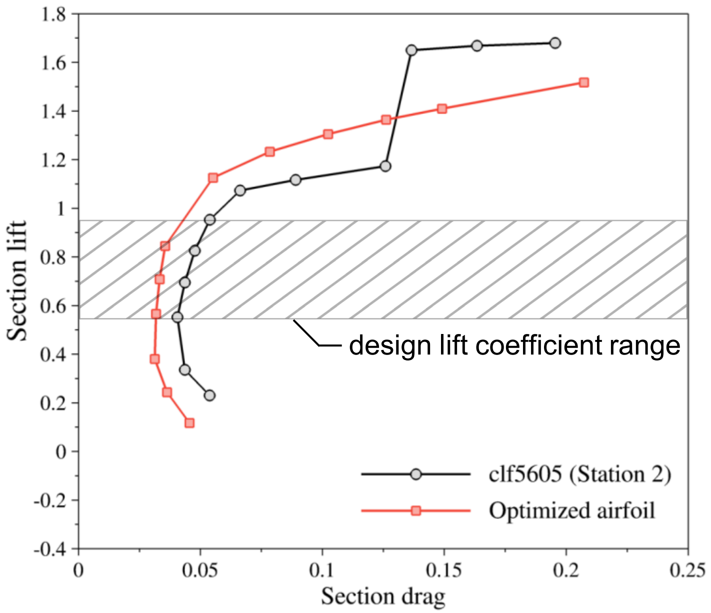

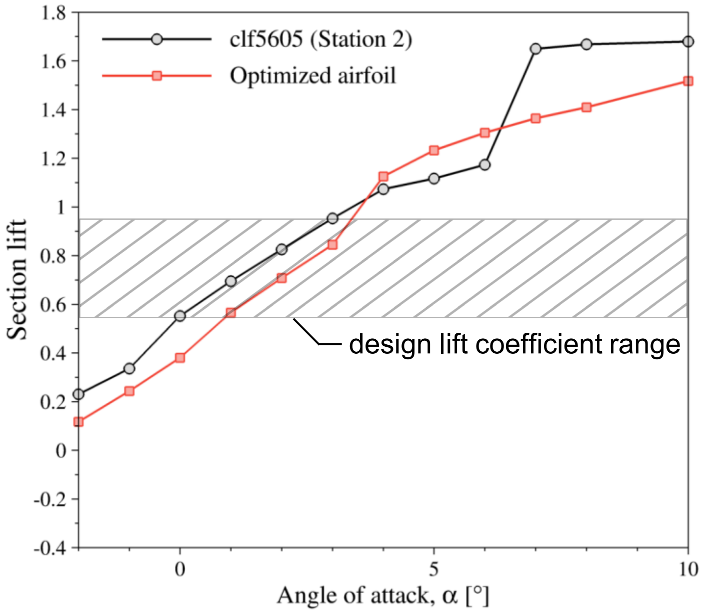

▲ Drag polar and lift curve for $Re = 14845$ and $M = 0.58$

Flow condition : $M = 0.70, Re = 14845$

Optimization Results

- **Station 3 ($r/R = 0.9241$)**
  - Optimized airfoil has a **thin-cambered shape**

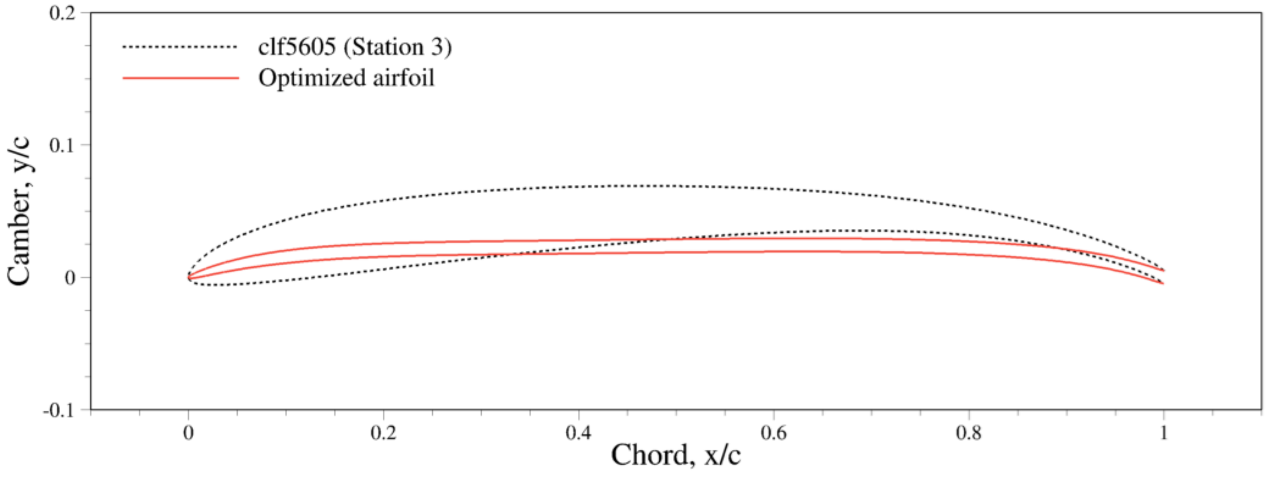

Performance	Fitness ($C_{d_{mean}}$*)	Improvement [%]
clf5605 (baseline)	**0.0517**	
Optimized airfoil	**0.0368**	**28.7**

Geometry	Max. Camber (f/c)	Max. Thickness (t/c)	Thickness (t/c) @ TE
clf5605 (baseline)	0.050	0.052	0.01
Optimized airfoil	0.025	0.010	0.01

*range of $C_{d_{mean}}$: $0.45 < C_l < 0.85$

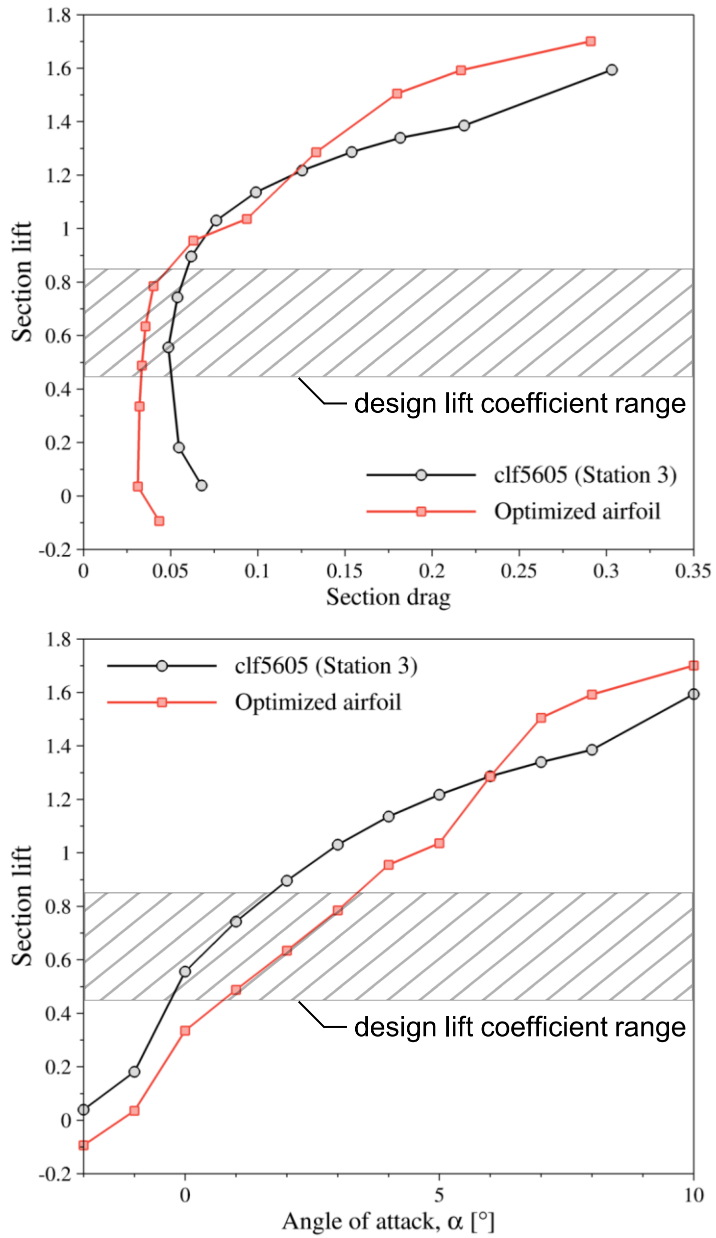

▲ Drag polar and lift curve for $Re = 12822$ and $M = 0.70$

Flow condition : $M = 0.70, Re = 12822$

Optimization Results

- **Station 3 ($r/R = 0.9241$)**

$C_l = 0.45$ | $C_l = 0.65$ | $C_l = 0.85$

clf5605 (baseline)

optimized airfoils

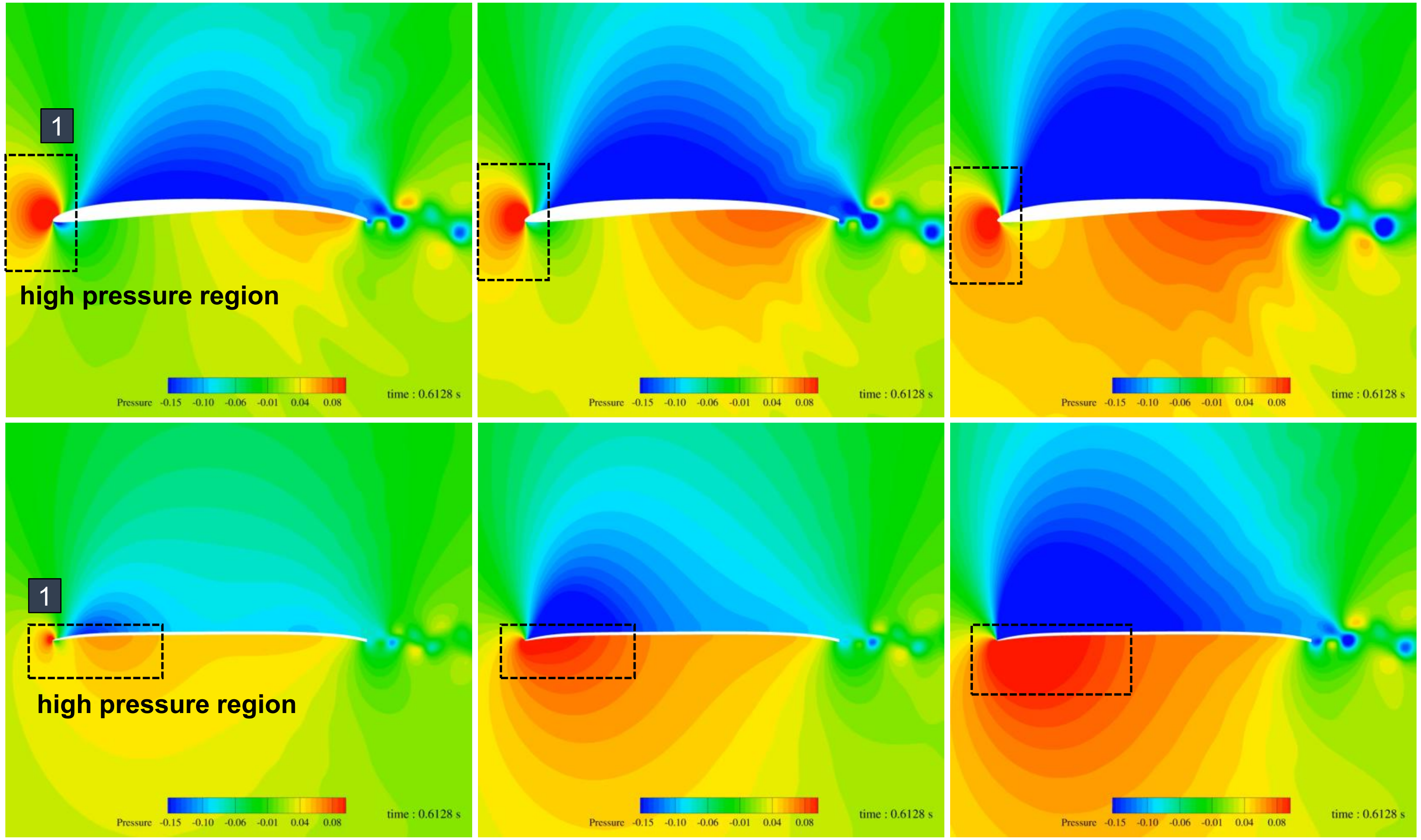

▲ Instantaneous flow field (non-dimensional gage pressure: $\Delta\bar{p} = \bar{p} - \bar{p}_\infty$)

1	High pressure region moves to pressure side from leading edge (∵ extremely-thin cambered airfoil effect) → reduce drag

⇒ ***Lower $C_{d_{pressure}}$***
(compared to baseline)

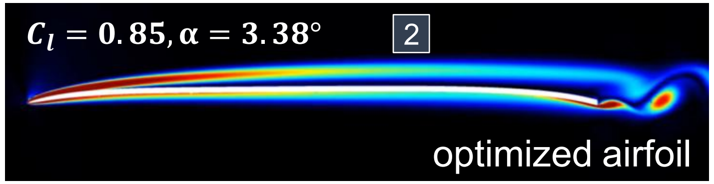

▲ Instantaneous flow field
(non-dimensional vorticity magnitude)

2	Absence of large-scale vortex shedding (∵ lower target C_l)

Flow condition : $M = 0.70, Re = 12822$

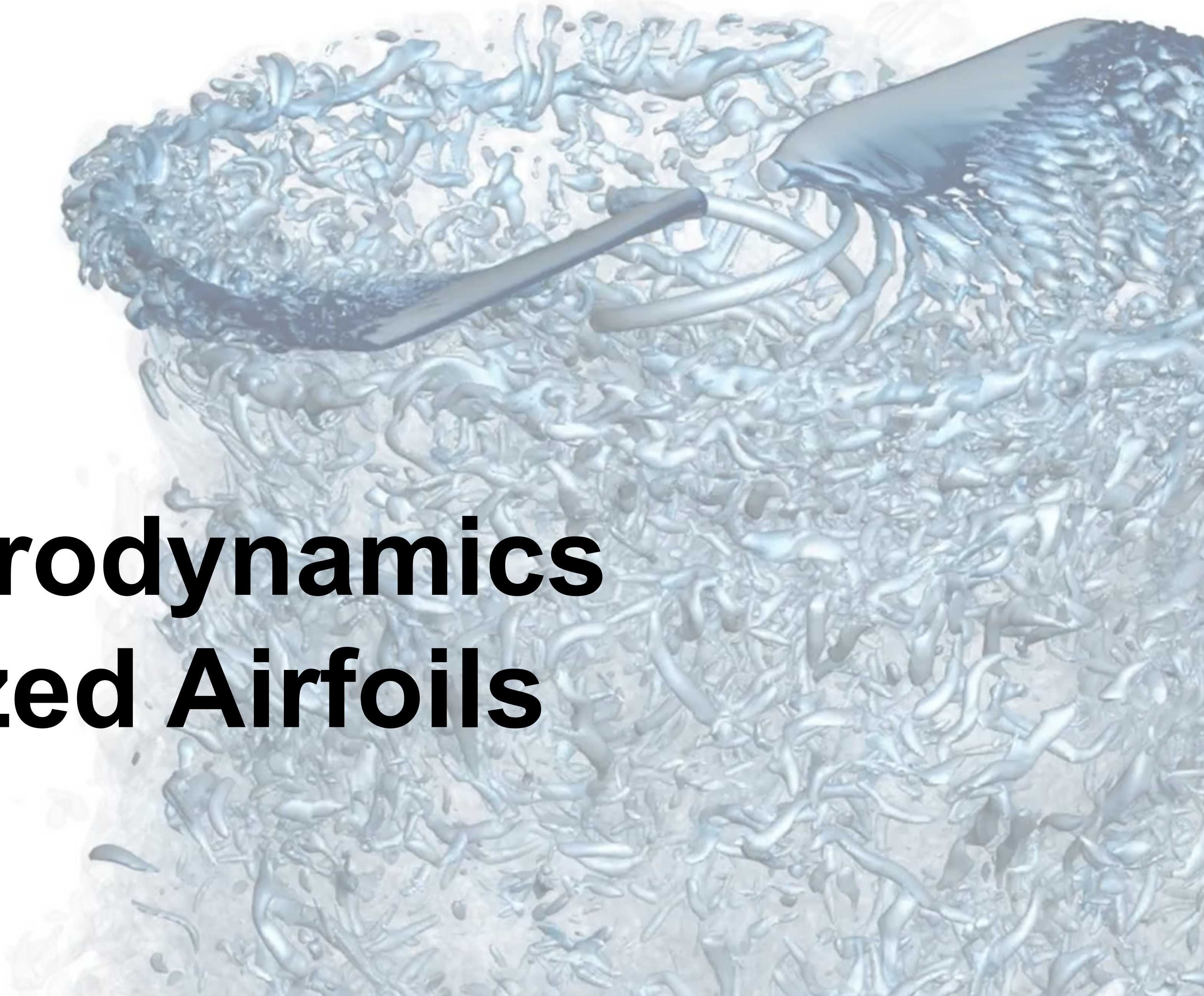

3D Rotor Aerodynamics with Optimized Airfoils

3D Rotor Aerodynamics with Optimized Airfoils

- Final Rotor Design with Optimized Airfoils

Top view

Front view

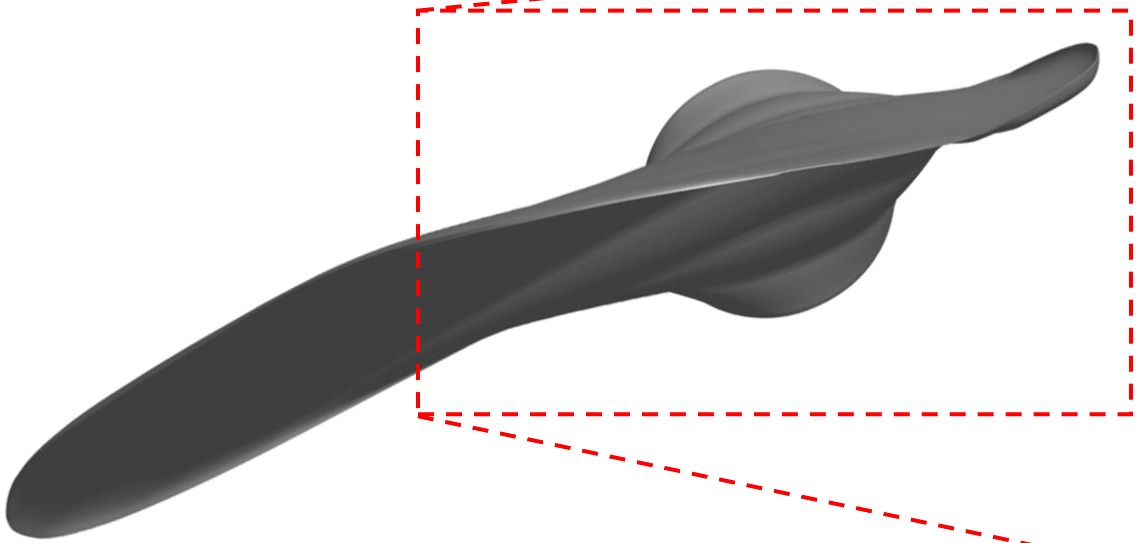

Side view

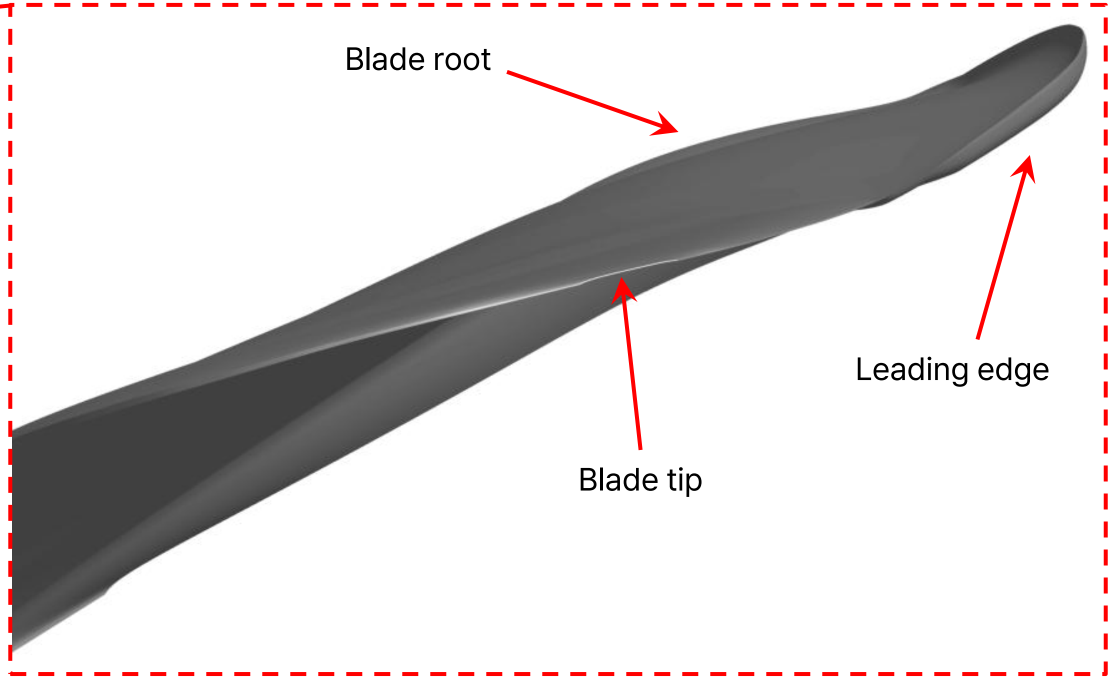

Flow condition : $M_{tip} = 0.76, Re = 21772$

3D Rotor Aerodynamics with Optimized Airfoils

- **3D Rotor Aerodynamics for design thrust condition**
  - **Baseline rotor** (Ingenuity single rotor) and **Optimized rotor** (airfoil optimized) are **trimmed** to match design thrust

$(C_T/\sigma = 0.125) \Rightarrow \quad FM_{baseline\ rotor} = 0.549,\ FM_{optimized\ rotor} = 0.588,\ \%\Delta FM = +6.9\%$

Averaged sectional load distribution

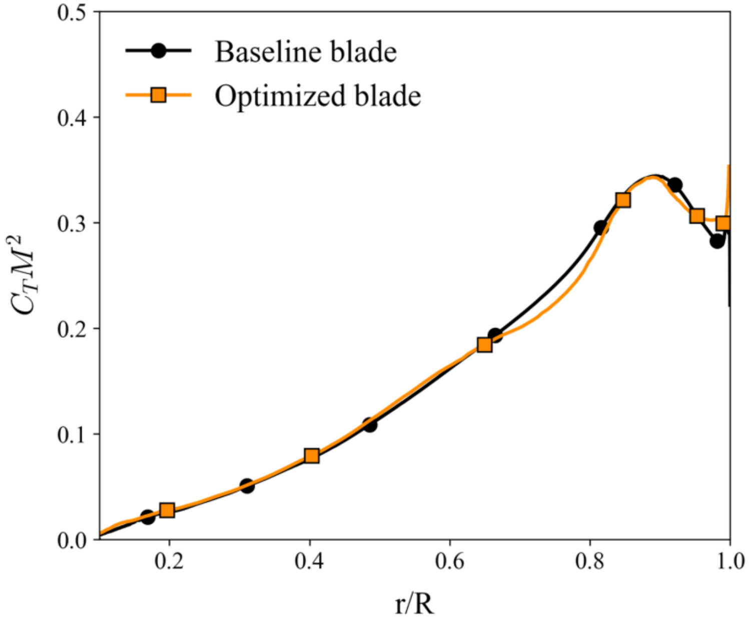

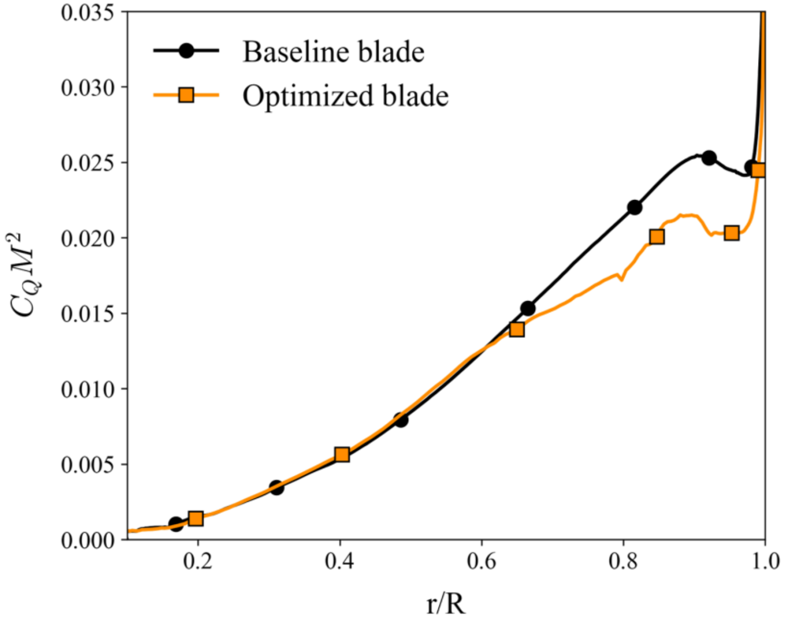

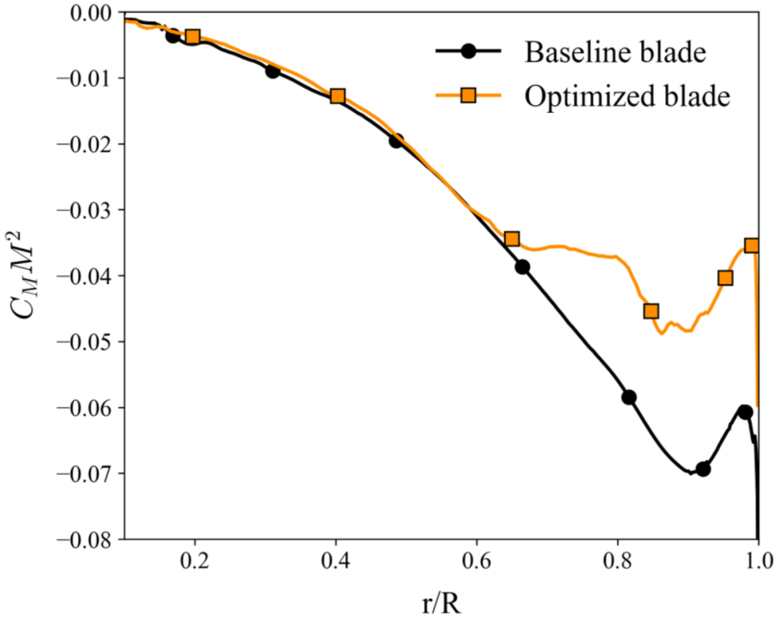

1 Both rotor have similar thrust distribution

2 Decreased sectional torque in optimized rotor at $r/R > 0.6$

3 Decreased sectional pitching moment in optimized rotor at $r/R > 0.6$

Aerospace Vehicle Design Laboratory

3D Rotor Aerodynamics with Optimized Airfoils

- **Comparing 2D and 3D Behavior of Optimized Airfoil**
  - **Station 2 ($r/R = 0.762$) :** 2D data is averaged for last 25 ctu and 3D data is averaged for last 1 rev

2D simulation

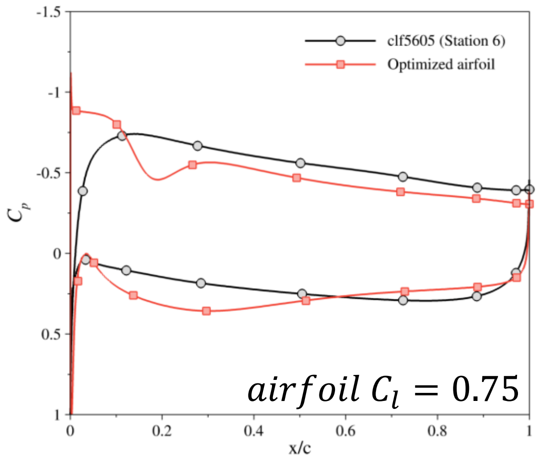

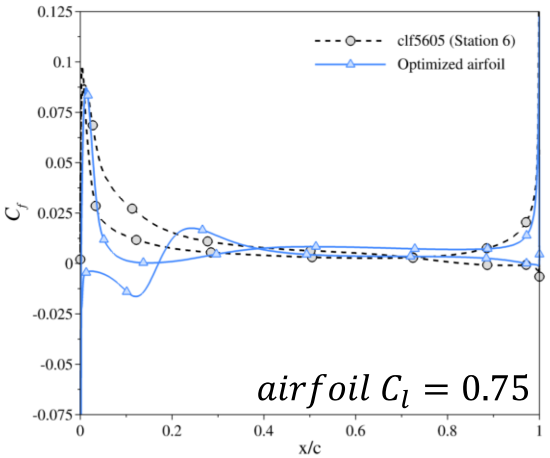

3D rotor simulation

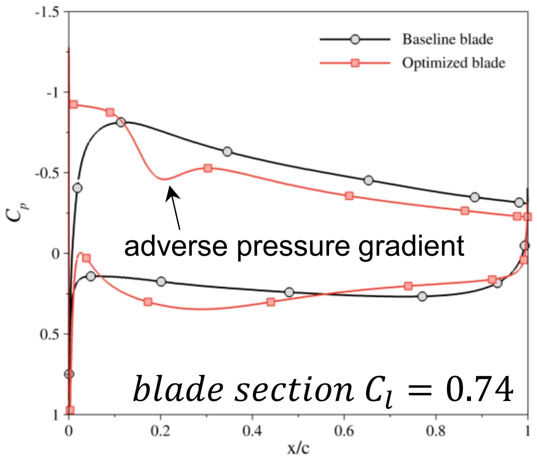

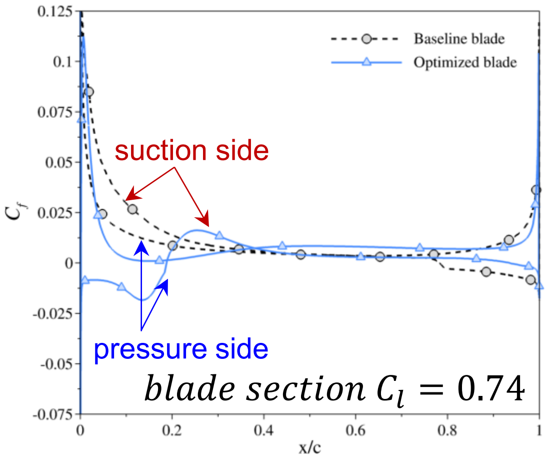

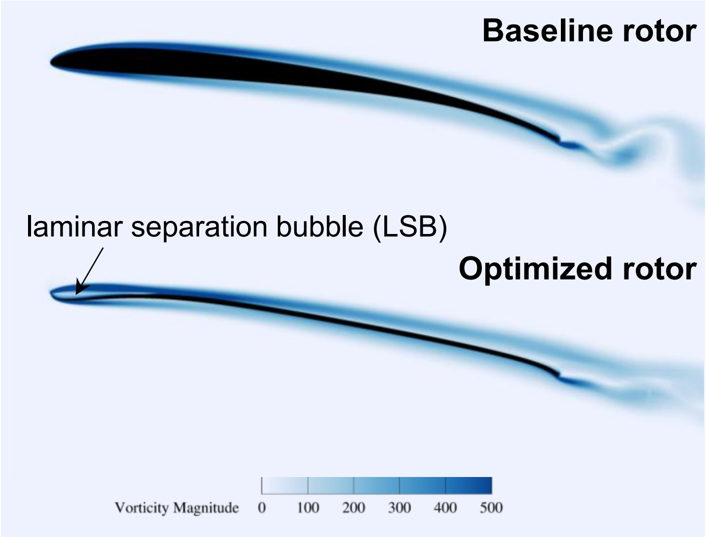

▲ Instantaneous flow field at $\psi = 0°$
(non-dimensional vorticity magnitude)

1	Exactly same pressure distribution and skin friction distribution are observed in 3D rotor

Flow condition : $M_{tip} = 0.76, Re = 21772$

3D Rotor Aerodynamics with Optimized Airfoils

- **Comparing 2D and 3D Behavior of Optimized Airfoil**
  - **Station 3 ($r/R = 0.9241$) :** 2D data is averaged for last 25 ctu and 3D data is averaged for last 1 rev

2D simulation | **3D rotor simulation**

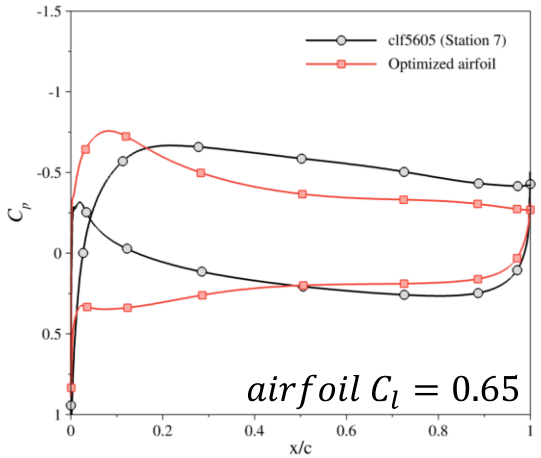

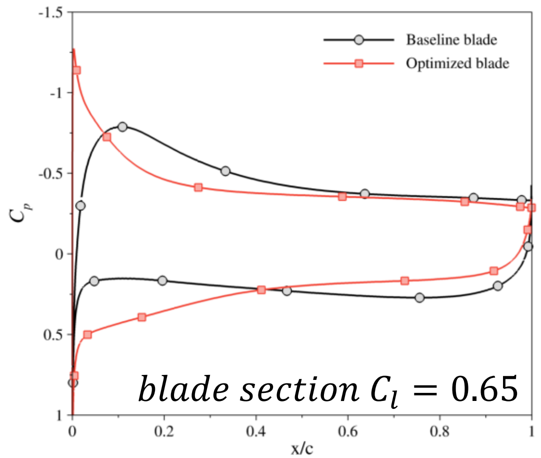

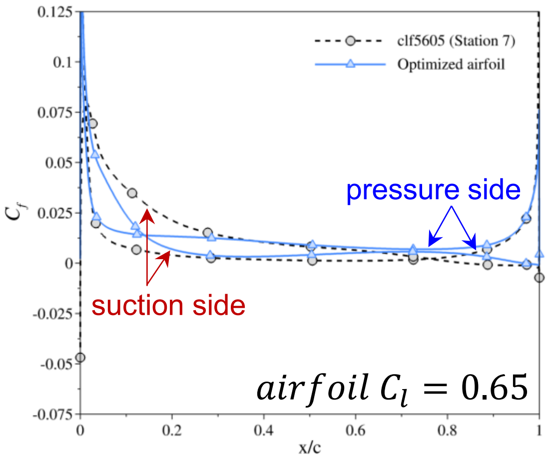

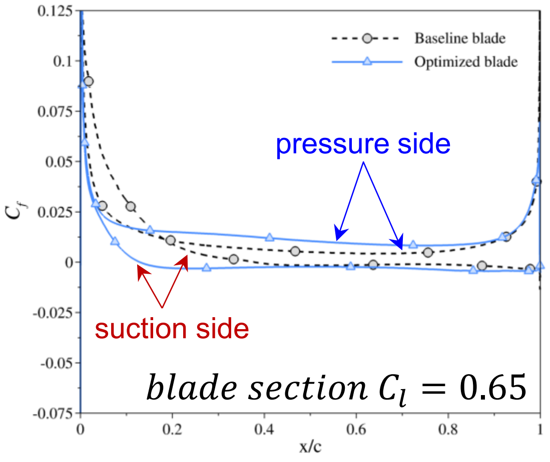

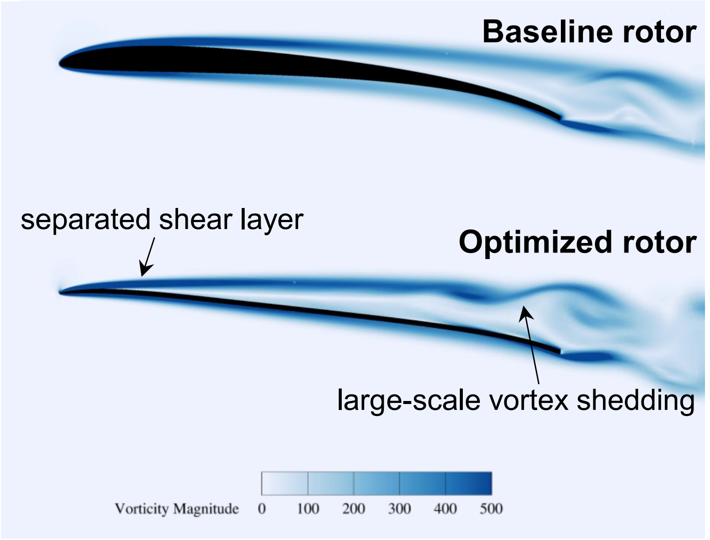

▲ Instantaneous flow field at $\psi = 0°$
(non-dimensional vorticity magnitude)

1	3D behavior is different with 2D behavior (onset of large-scale vortex shedding in 3D)
2	Skin friction at suction side decreased in 3D rotor

Q-criterion

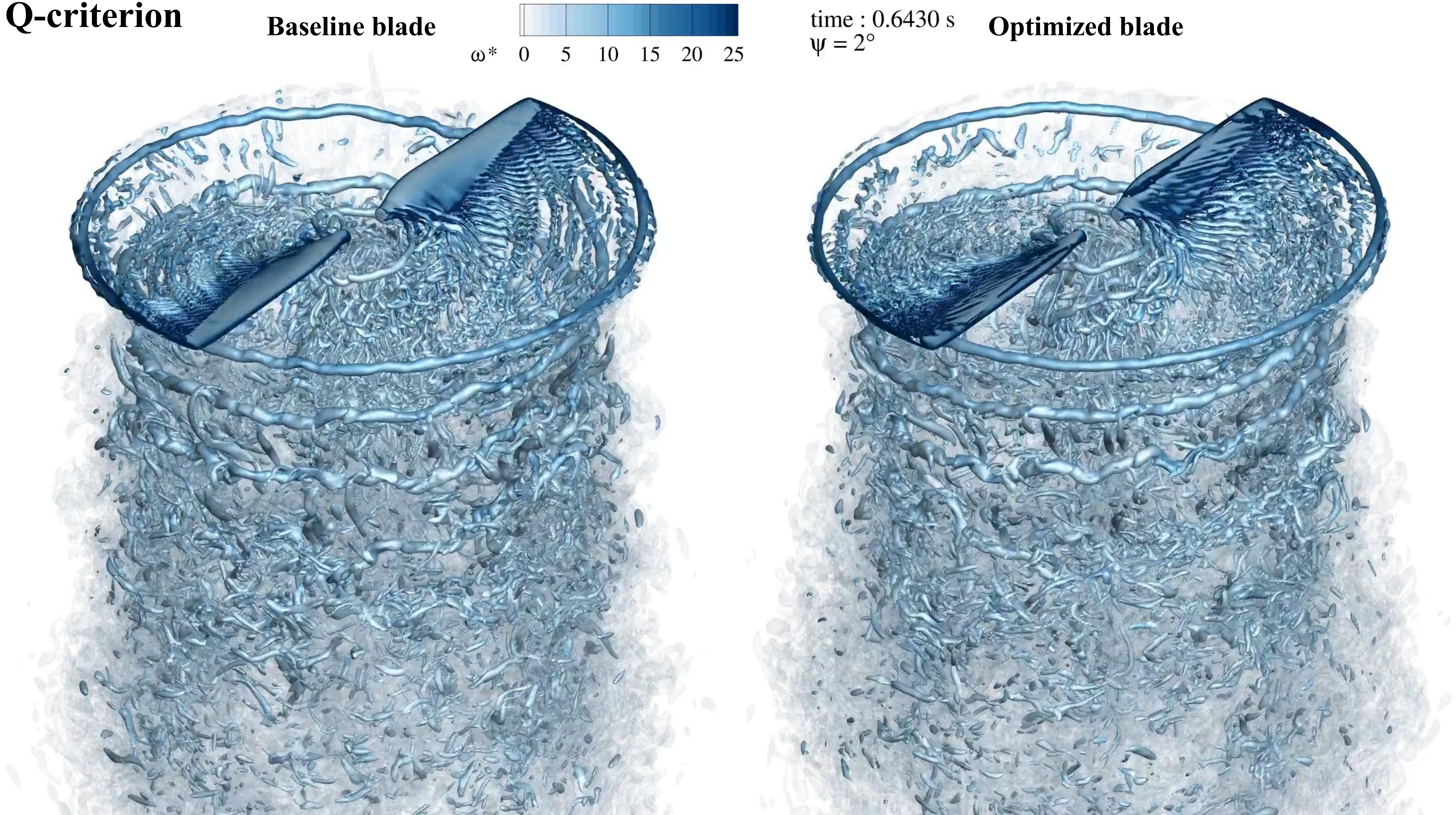

Baseline blade
ω*
0
5
10
15
20
25
time : 0.6430 s
ψ = 2°
Optimized blade

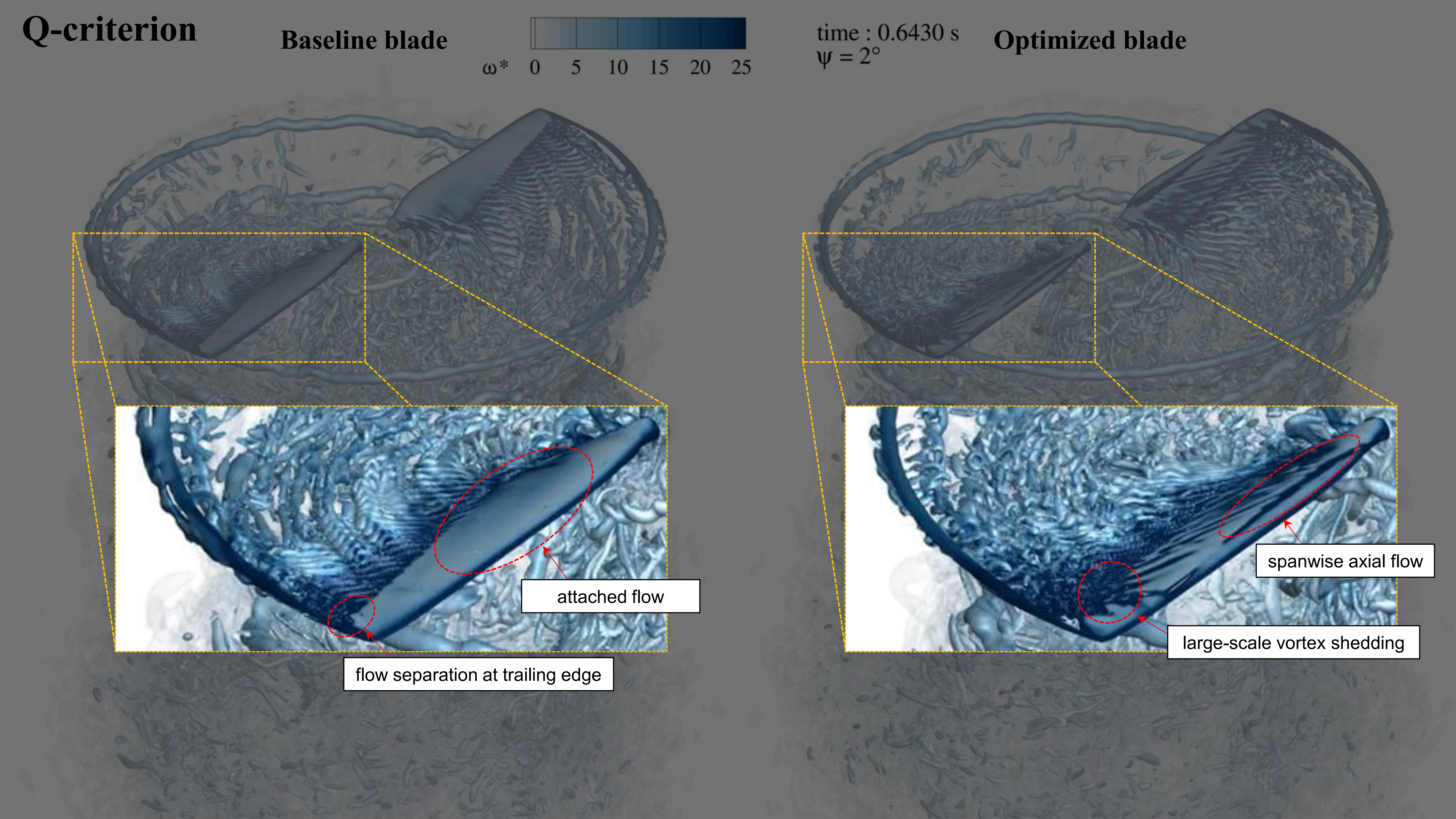
Q-criterion
Baseline blade
ω*
0
5
10
15
20
25
time : 0.6430 s
ψ = 2°
Optimized blade
attached flow
flow separation at trailing edge
spanwise axial flow
large-scale vortex shedding

Flow condition : $M_{tip} = 0.76, Re = 21772$

3D Rotor Aerodynamics with Optimized Airfoils

- **Off-Design Analysis Results**
  - Overall performance of **baseline rotor (Ingenuity single rotor)** and **optimized rotor (airfoil optimized)**

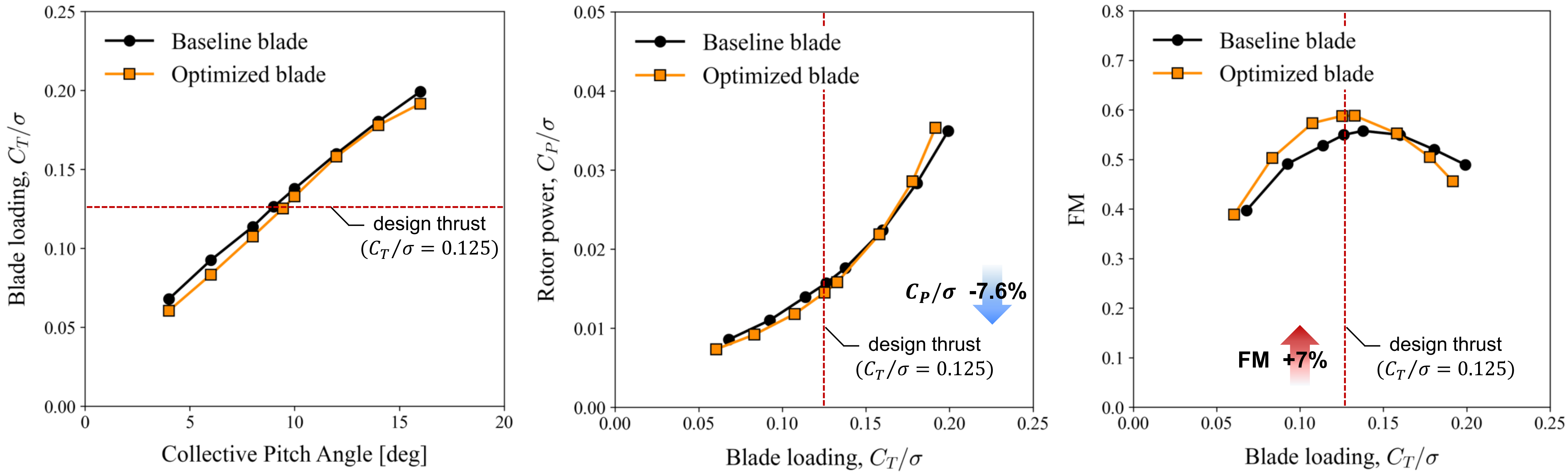

1 Less thrust at the same collective pitch (∵ reverse camber effect)

2 Figure of Merit increased about 7% near the design thrust

3 Margin between the design thrust and the maximum FM is decreased (∵ earlier onset of stall)

Flow condition : $M_{tip} = 0.76, Re = 21772$

3D Rotor Aerodynamics with Optimized Airfoils

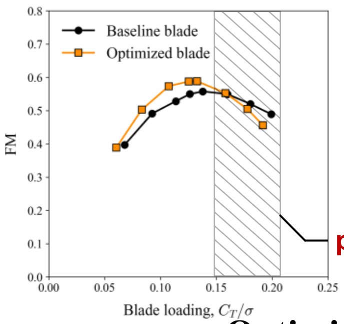

- **Off-Design Analysis Results (Post-stall range)** * Instantaneous flow field

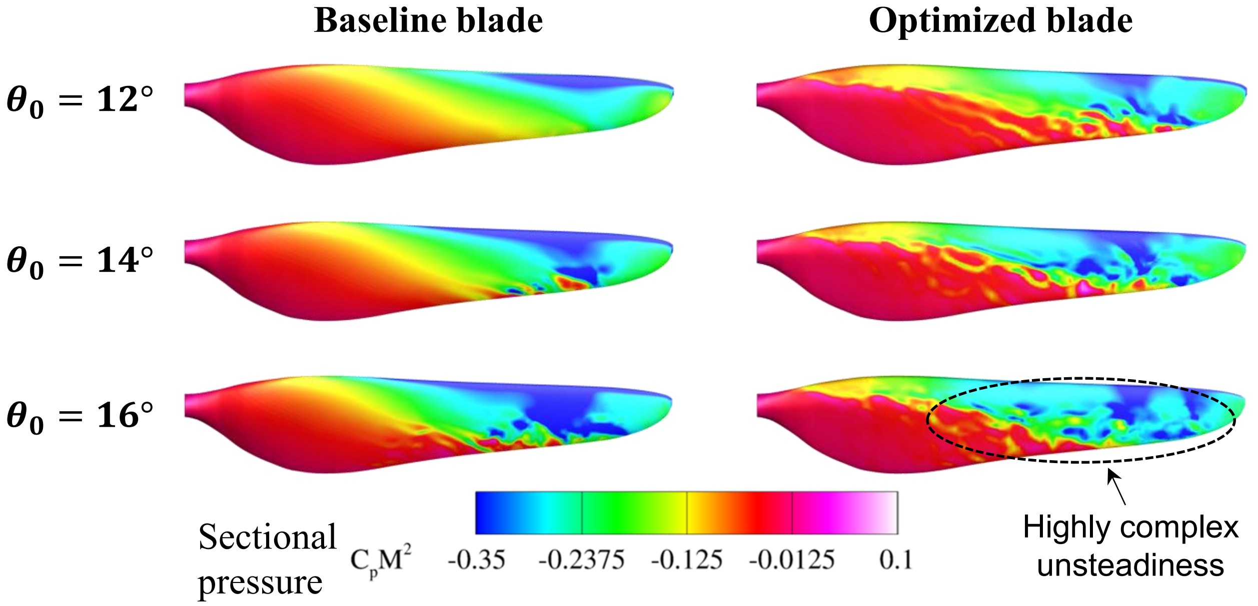

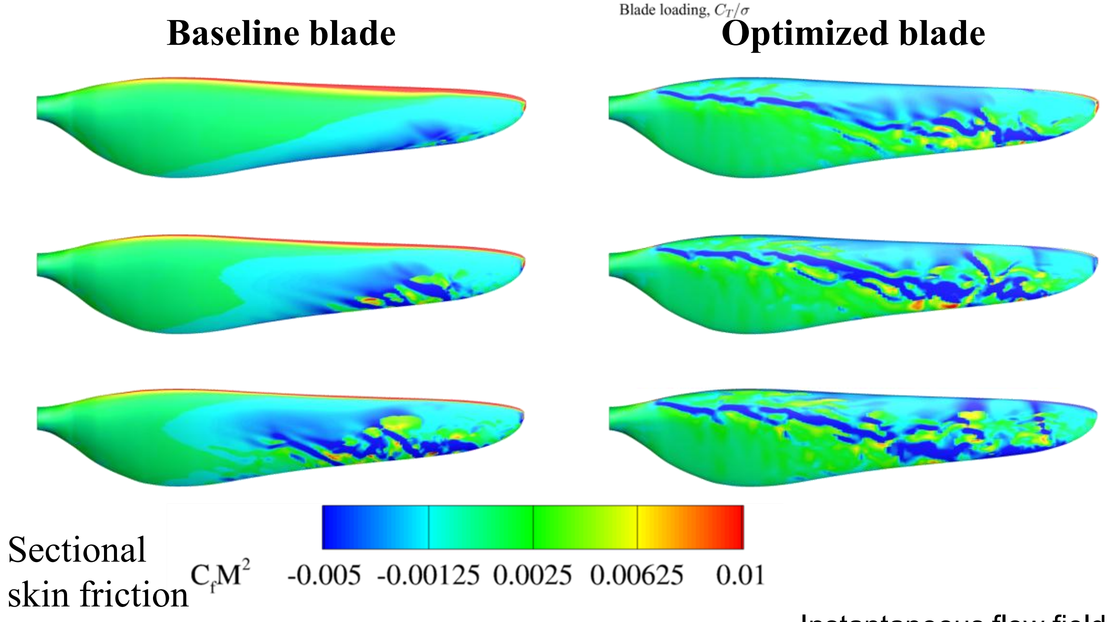

Instantaneous flow field

1	Optimized blade is underperforming the baseline over the $\theta_0 = 10°\sim16°$ range

2	Highly complex unsteadiness and increased skin friction are observed in optimized rotor at every pitch angle

Conclusion

Conclusion

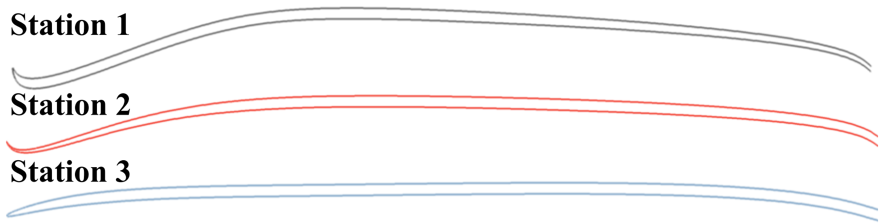

- **Derived high-performance airfoils for three different stations**
  - The drag of each optimized airfoil is **reduced by 21–28%** and compared to the baseline under the same C_l condition
- **Identified the mechanism behind the superior aerodynamic performance of Sharp Raised-lip (SRL) airfoil and thin cambered airfoil**
  - The SRL forces shear layer separation from the leading edge (LE), generating a LE laminar separation bubble (LSB)
  - Shear layer separation and LSB contribute positively to aerodynamic performance, as they **reduce skin friction drag**, which accounts for 10–50% of total drag in low Reynolds number conditions
- **Explored rotor aerodynamics and airfoil behavior in a 3D rotor**
  - Identified optimized performance within the pre-stall range, with a 7% increase in FM at the design thrust condition
  - **Stations 3 exhibits different aerodynamic characteristics to 2D airfoil,** while station 1 and 2 show similarity
- **Future work**
  - Iterative airfoil design optimization considering 3D effect in the blade tip section
  - Verify manufacturability and design feasibility for the forward flight condition

Thank you for your attention

Contact info:

Seongjoong Park

eric2237@snu.ac.kr

This research was supported by the German Aerospace Center's (DLR) high-performance computing resources.

SEOUL NATIONAL UNIVERSITY
AEROSPACE VEHICLE DESIGN LABORATORY

Appendix

[1] Munday, P. M., Taira, K., Suwa, T., Numata, D., and Asai, K., "Nonlinear lift on a triangular airfoil in low-Reynolds-number compressible flow," Journal of Aircraft, vol. 52, 2015, pp. 924–931.
[2] Koning, W. J. F., Romander, E. A., and Johnson, W., "Optimization of Low Reynolds Number Airfoils for Martian Rotor Applications Using an Evolutionary Algorithm," AIAA Science and Technology Forum and Exposition (AIAA SciTech), AIAA Paper 2020-0084, 2020, Orlando, FL, U.S.A., January 2020.
[3] Caros, L., Buxton, O., Shigeta, T., Nagata, T., Nonomura, T., Asai, K., and Vincent, P., "Direct Numerical Simulation of Flow over a Triangular Airfoil Under Martian Conditions," AIAA Journal, Vol. 60, No. 7, 2022, pp. 20[illegible]–2072.

Description of 2D Validation Case

- **Triangular airfoil**
  - Experiment data: Triangular airfoil test in the Mars Wind Tunnel (MWT) at Tohoku University (test section: 400 mm in length, 150 mm in height, and 100 mm in width) [1]
  - CFD data : Unsteady RANS (OVERFLOW) [2] / ILES (PyFR) [3]

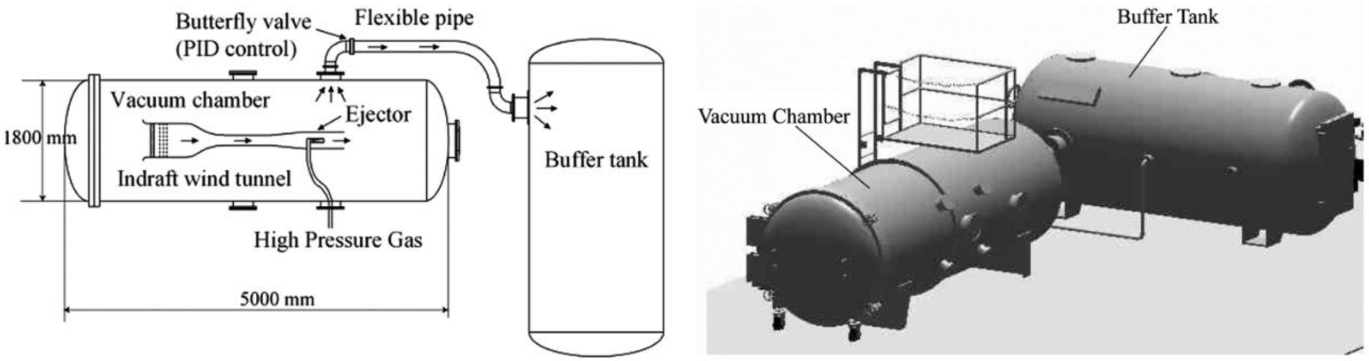

▲ MWT at Tohoku University. Schematic of the MWT interior (left) and exterior (right)[1]

Variable	Mars Wind Tunnel
Reynolds number	3000
Mach number	0.15, 0.5
Specific heat ratio, γ	1.4
Prandtl number	0.71

▲ Flow condition of experiment and CFD simulations

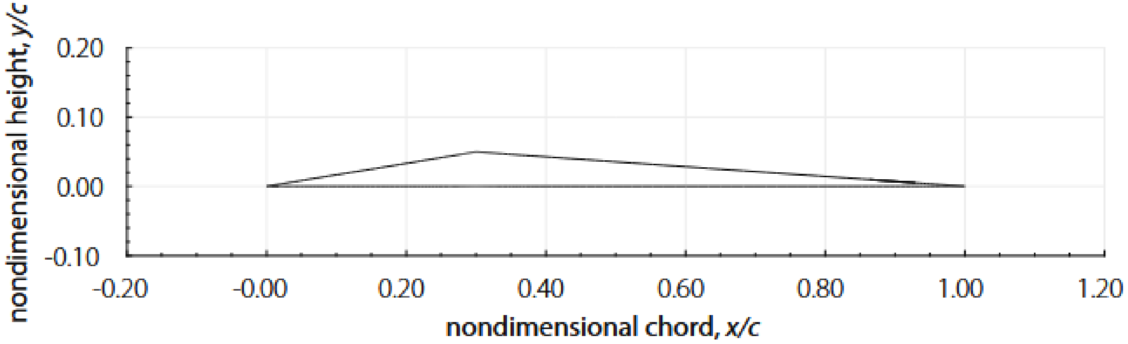

▲ Triangular airfoil geometry

Aerospace Vehicle Design Laboratory

2D Numerical Simulation Setup

- **2D Grid Refinement Study**
  - Grid refinement study performed for $\alpha = 12°$ at M=0.15, Re=3000
  - Calculated difference:

$$\Delta C_l = \left|C_l - C_{l,fine}\right| / C_{l,fine}$$

Grid size	C_l	ΔC_l [%]	C_d	ΔC_d [%]
Fine (20.6 × 10^4)	1.249	-	0.2768	-
Medium (7.3 × 10^4)	1.252	**0.253**	0.2762	**0.196**
Coarse (1.8 × 10^4)	1.238	1.100	0.2756	0.121
Very Coarse (0.5 × 10^4)	1.185	4.268	0.2610	5.284

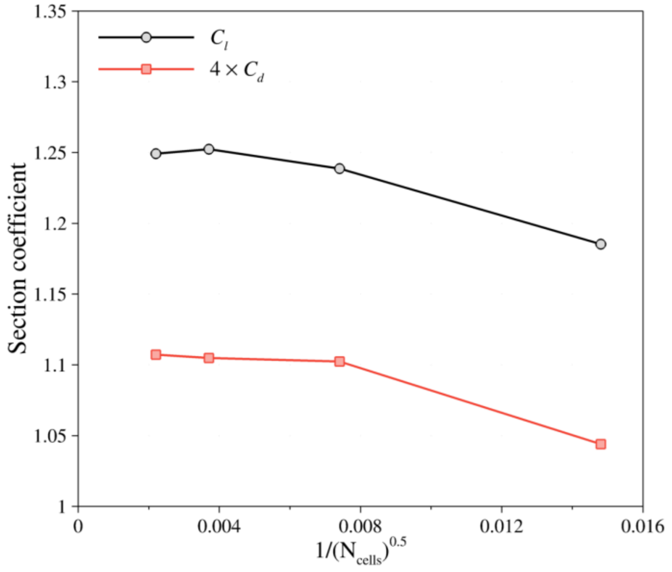

  - **Medium-resolution grid** $(n_x = 609, n_y = 120)$ has sufficient grid resolution
    → selected as typical grid used for 2D simulation

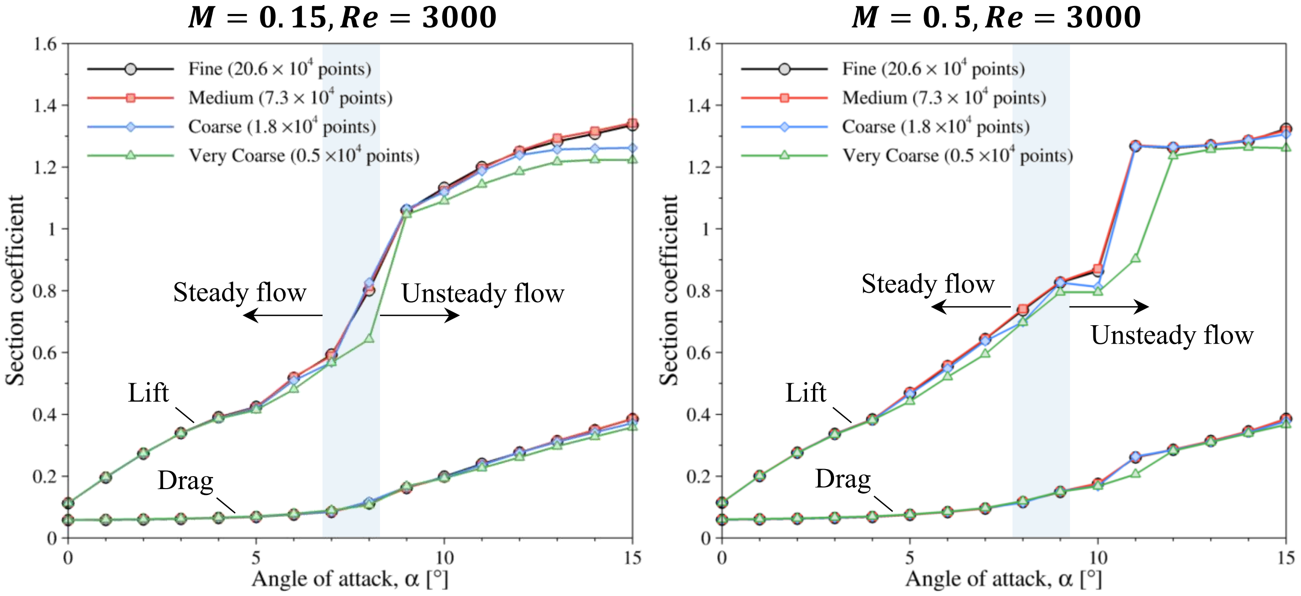

▲ Grid refinement study for $\alpha = 0° \sim 15°$

[1] Koning, W. J. F., Allan, B. G., Romander, E. A., and Johnson, W., "Comparing 3D and 2D CFD for Mars Helicopter Ingenuity Rotor Performance Prediction," presented at the 49th European Rotorcraft Forum 2023, Bückeburg, 2023.
[2] Koning, W. J. F., and Dominguez, M., "Mars Helicopter Ingenuity Rotor Geometry," NASA/TM-20240001510, Ames Research Center, Moffett Field, California, 2024.

Description of 3D Validation Case

- **Transonic Rotor Test (TRT)**
  - Experiment data: Transonic Rotor Test (TRT) at the JPL Space Simulator (JPLSS) using CO2 as the driving gas [1]
    (Experiment rotor is a single rotor from NASA's Ingenuity Mars helicopter)
  - CFD data: Laminar UNS 3D OVERFLOW (Koning, W.J.F. et al. [1])

▲ NASA's Ingenuity Mars Helicopter (NASA/JPL-Caltech)

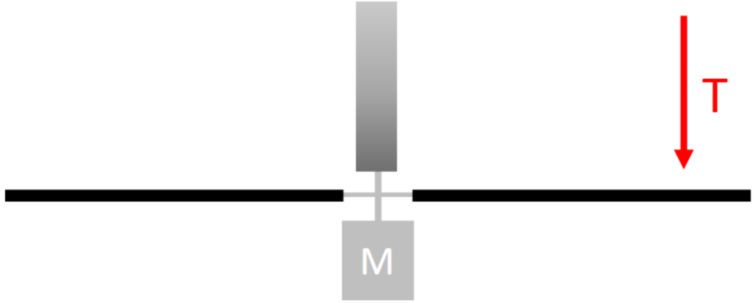

▲The schematic experimental setup for the TRT test in the JPL Space Simulator

validation condition

TRT condition	1	2	3	4	5
M_{tip}	0.65	0.70	0.75	0.80	0.85
RPM	2,740	2,950	3,160	3,375	,3585

▲ TRT Test Conditions

Variable	Earth (SLS)	TRT
Density, ρ [kg/m^3]	1.225	0.01
Temerature, T [K]	288.2	293.15
Gas constant, R [m^2 /s^2 /K]	287.1	188.9
Specific heat ratio, γ	1.4	1.289
Dynamic viscosity, μ [N·s/m^2]	$1.75 \cdot 10^{-5}$	$1.46 \cdot 10^{-5}$
Speed of sound, a [m/s]	340.35	267.17

▲ Approximate JPLSS Test Conditions with Earth sea-level Standard (SLS) conditions

[1] Koning, W. J. F., Allan, B. G., Romander, E. A., and Johnson, W., "Comparing 3D and 2D CFD for Mars Helicopter Ingenuity Rotor Performance Prediction," presented at the 49th European Rotorcraft Forum 2023, Bückeburg, 2023.
[2] Koning, W. J. F., and Dominguez, M., "Mars Helicopter Ingenuity Rotor Geometry," NASA/TM-20240001510, Ames Research Center, Moffett Field, California, 2024.

Description of 3D Validation Case

- **Transonic Rotor Test (TRT)**
  - Rotor geometry : extracted from the OML CAD model of Ingenuity's rotor blades

Parameter	Value
Rotor radius, R [m]	1.225
Disk area, A [m^2]	288.2
Blade area [m^2]	0.085
Solidity (thrust-weighted), σ	0.07391
Design RPM	2600

▲Specification of single rotor from Ingenuity [1]

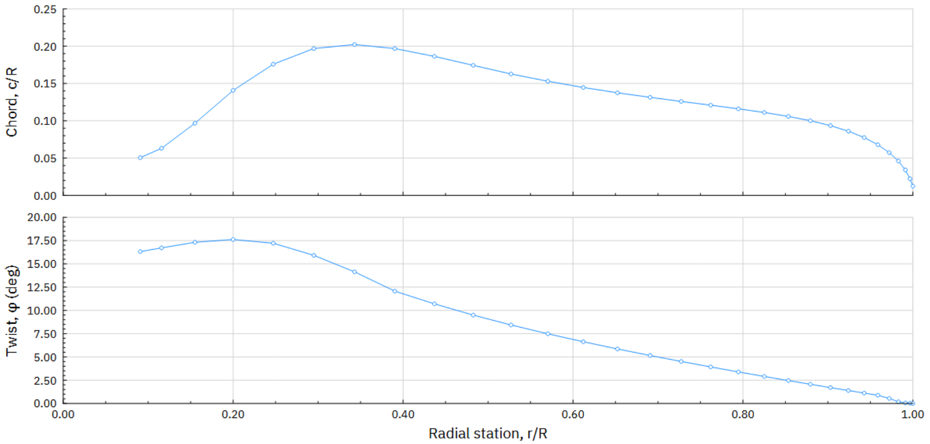

▲Rotor chord and twist distribution [1]

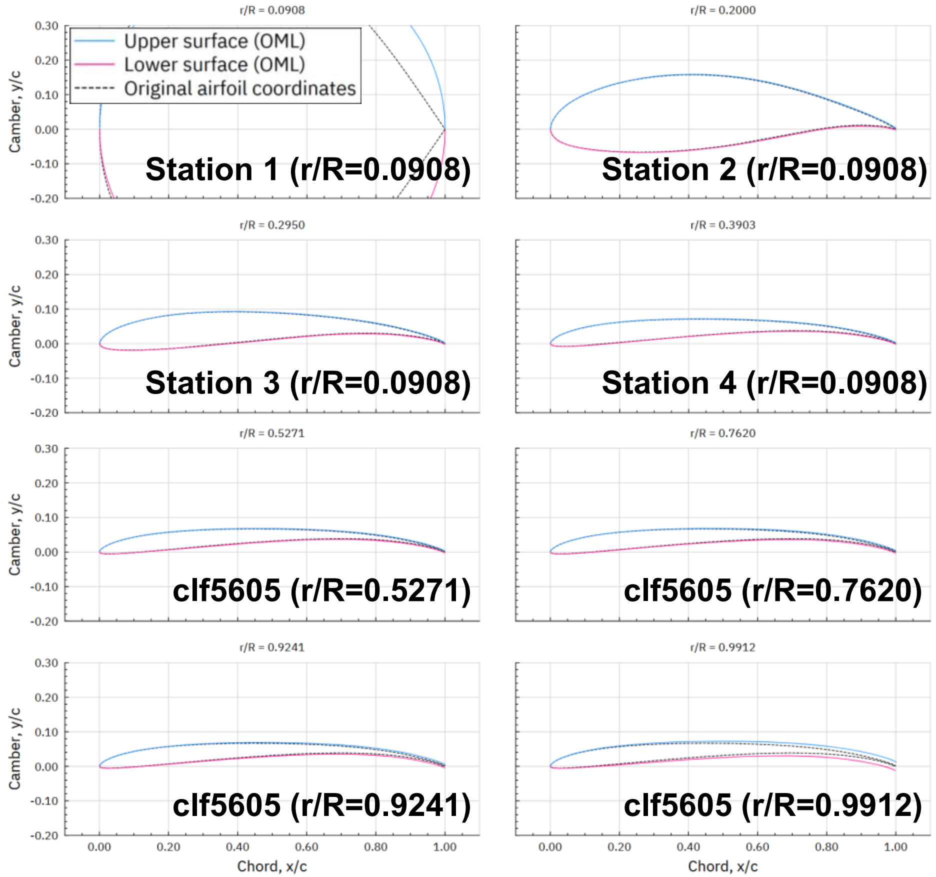

▲ Normalized OML airfoil profiles for 8 representative radial stations [1]

Ingenuity has 5 airfoils (Station 1~4, clf5605)

trailing edge thickness modified to around 0.5 mm (∵ manufacturability limits and structural constraints)

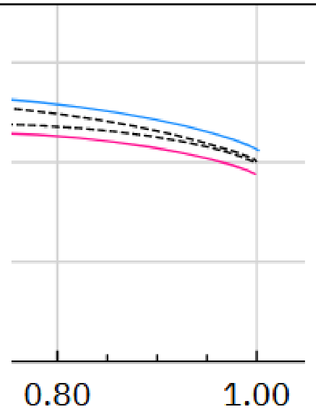

→ Using OML profiles for CFD simulation

3D Numerical Simulation Setup

- **3D Rotor Grid Refinement Study**
  - Grid refinement study performed for $\theta_0 = 14°$
  - Calculated difference:

$$\Delta C_T/\sigma = |C_T/\sigma - C_{T,fine}/\sigma|/(C_{T,fine}/\sigma)$$

Grid size	C_T/σ	$\Delta C_T/\sigma$ [%]	C_P/σ	$\Delta C_P/\sigma$[%]
*Fine (676.0 × 10^6)	0.170	-	0.0275	-
Medium (84.5 × 10^6)	0.169	0.159	0.0275	0.120
Coarse (10.5 × 10^6)	0.168	1.110	0.0273	0.678
Very Coarse (1.3 × 10^6)	0.161	5.097	0.0264	3.824

* Coefficients for fine grid are extrapolated using Richardson method

  - **Medium-resolution grid** (84.5 M points) has sufficient grid resolution
    → selected as typical grid used for 3D rotor simulation

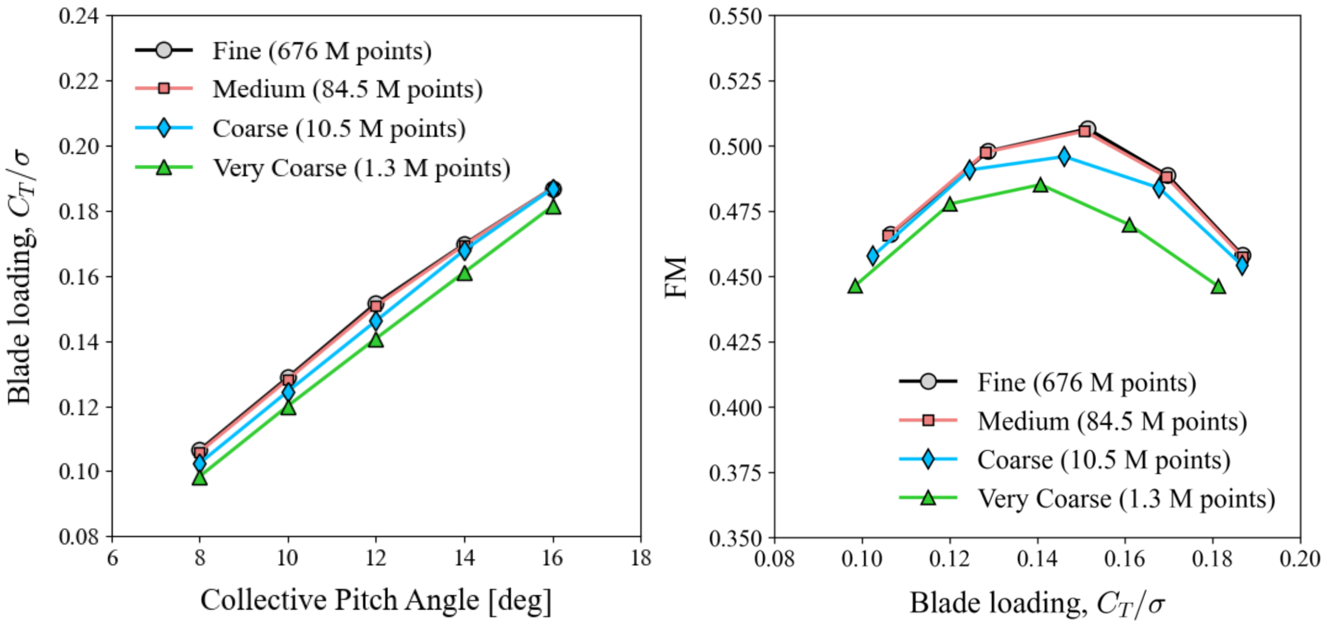

▲ Grid refinement study for $\theta_0 = 8°\sim16°$

[1] Lu, X., Huang, J., Song, L., and Li, J., "An Improved Geometric Parameter Airfoil Parameterization Method," Aerospace Science and Technology, Vol. 78, 2018, pp. 241–247.
[2] Wilke, G., "AFRO (Airfoils for Rotor Optimization)"

Optimization Framework

- **Parameterization Method**
  - Improved geometric parameterization (IGP) with *NURBS [1, 2]
    - ✓ Camber line expressed by NURBS with 6 control points : $c_i(x_i, y_i)$
    - ✓ Thickness line expressed by NURBS with 6 control points : $t_i(x_i, y_i)$

Control point	Variable	Value
c_0	x_0	0.0
	y_0	0.0
$\boldsymbol{c_1}$	$\boldsymbol{x_1}$	$\boldsymbol{DV_1}$
	$\boldsymbol{y_1}$	$\boldsymbol{DV_2}$
$\boldsymbol{c_2}$	$\boldsymbol{x_2}$	$\boldsymbol{DV_3}$
	$\boldsymbol{y_2}$	$\boldsymbol{DV_4}$
$\boldsymbol{c_3}$	$\boldsymbol{x_3}$	$\boldsymbol{DV_5}$
	y_3	$y_3 = y_2$
$\boldsymbol{c_4}$	$\boldsymbol{x_4}$	$\boldsymbol{DV_6}$
	$\boldsymbol{y_4}$	$\boldsymbol{DV_7}$
c_5	x_5	1.0
	y_5	0.0

▲ Definition of control points for **camber**

Control point	Variable	Value
t_0	x_0	0.0
	$\boldsymbol{y_0}$	$\boldsymbol{DV_8}$
$\boldsymbol{t_1}$	$\boldsymbol{x_1}$	$\boldsymbol{DV_9}$
	y_1	0.01
t_2	x_2	$x_2 = x_1 + 0.05$
	y_2	0.01
t_3	x_3	$x_3 = x_4 - 0.05$
	y_3	0.01
$\boldsymbol{t_4}$	$\boldsymbol{x_4}$	$\boldsymbol{DV_{10}}$
	y_4	0.01
t_5	x_5	1.0
	y_5	0.0

▲ Definition of control points for **thickness**

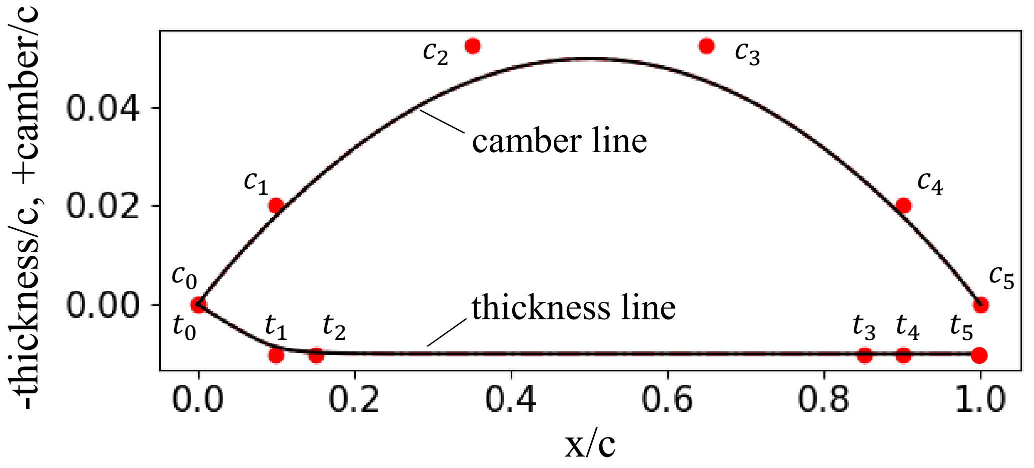

▲ Definition of NURBS for decoupled camber and thickness

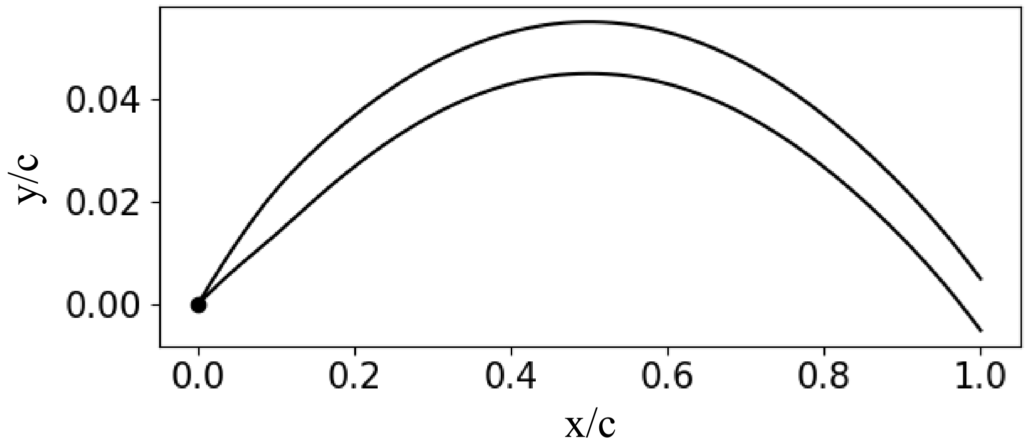

▲ **5% cambered plate airfoil** geometry generated by IGP with NURBS

*NURBS: Non-uniform rational B-spline